



1 **An evaluation of new particle formation events in Helsinki during a Baltic Sea cyanobacterial**
2 **summer bloom**

3
4 Roseline C. Thakur¹, Lubna Dada^{1,2,3}, Lisa J. Beck¹, Lauriane L.J. Quéléver¹, Tommy Chan¹, Marjan
5 Marbouti¹, Xu-Cheng He¹, Carlton Xavier¹, Juha Sulo¹, Janne Lampilahti¹, Markus Lampimäki¹, Yee
6 Jun Tham^{1,11}, Nina Sarnela¹, Katrianne Lehtipalo^{1,4}, Alf Norkko^{8,9}, Markku Kulmala^{1,5,6,7}, Mikko
7 Sipilä¹, Tuija Jokinen^{1,10}

8
9 ¹Institute for Atmospheric and Earth System Research/Physics, Faculty of Science, 00014 University
10 of Helsinki, Helsinki, Finland.

11 ²School of Architecture, Civil and Environmental Engineering, École Polytechnique Fédérale de
12 Lausanne, Lausanne, Switzerland

13 ³Laboratory of Atmospheric Chemistry, Paul Scherrer Institute, 5232 Villigen PSI, Switzerland

14 ⁴Finnish Meteorological Institute, Helsinki, Finland.

15 ⁵Aerosol and Haze Laboratory, Beijing Advanced Innovation Center for Soft Matter Science and
16 Engineering, Beijing University of Chemical Technology, 100089 Beijing, China.

17 ⁶Joint International Research Laboratory of Atmospheric and Earth System Sciences, Nanjing
18 University, 210023 Nanjing, China.

19 ⁷Lomonosov Moscow State University, Faculty of Geography, 119991, Moscow, GSP-1, 1
20 Leninskiye Gory.

21 ⁸Tvärminne Zoological Station, University of Helsinki, J.A. Palméns väg 260, FI-10900 Hangö,
22 Finland

23 ⁹Baltic Sea Centre, Stockholm University, Stockholm, Sweden

24 ¹⁰Climate & Atmosphere Research Centre (CARE-C), The Cyprus Institute, P.O. Box 27456, Nicosia,
25 CY-1645, Cyprus.

26 ¹¹School of Marine Sciences, Sun Yat-Sen University, Zhuhai 519082, China

27
28
29 Correspondence to: roseline.thakur@helsinki.fi

30 **Abstract**

31 Several studies have investigated New Particle Formation (NPF) events from various sites ranging
32 from pristine locations, including (boreal) forest sites to urban areas. However, there is still a dearth
33 of studies investigating NPF processes and subsequent aerosol growth in coastal yet semi-urban sites,
34 where the tropospheric layer is a concoction of biogenic and anthropogenic gases and particles. The
35 investigation of factors leading to NPF becomes extremely complex due to the highly dynamic
36 meteorological conditions at the coastline especially when combined with both continental and
37 oceanic weather conditions. Herein, we engage a comprehensive study of particle number size
38 distributions and aerosol-forming precursor vapors at the coastal semi-urban site in Helsinki, Finland.
39 The measurement period, 25 June 2019–18 August 2019, was timed with the recurring cyanobacterial
40 summer bloom in the Baltic Sea region and coastal regions of Finland. Our study recorded several
41 regional/local NPF and aerosol burst events during this period. Although the overall anthropogenic
42 influence on Sulfuric Acid (SA) concentrations was low during the measurement period, we observed
43 that the regional or local NPF events, characterized by SA concentrations in the order of 10⁷



44 molecules per cm^{-3} occurred mostly when the air mass travelled over the land areas. Interestingly,
45 when the air mass travelled over the Baltic Sea, an area enriched with Algae and cyanobacterial
46 blooms, high Iodic Acid (IA) concentration coincided with an aerosol burst or a spike event at the
47 measurement site. Further, SA-rich bursts were seen when the air mass travelled over the Gulf of
48 Bothnia, enriched with cyanobacterial blooms. The two most important factors affecting aerosol
49 precursor vapor concentrations, and thus the aerosol formation, were (1) the type of phytoplankton
50 species and intensity of bloom present in the coastal regions of Finland/ Baltic Sea and (2) the wind
51 direction. During the events, most of the growth of sub-3 nm particles was probably due to SA, rather
52 than IA or MSA, however much of the particle growth remained unexplained indicative of the strong
53 role of organics in the growth of particles, especially in the 3–7 nm particle size range. Further studies
54 are needed to explore the role of organics in NPF events and the potential influence of cyanobacterial
55 blooms in coastal locations.

56

57 Keywords: coastal environment, particle growth, methane sulfonic acid, cyanobacterial summer
58 bloom, sulfuric acid, iodic acid

59

60 **1 Introduction**

61 New particle formation (NPF) and growth of aerosols are regional processes occurring globally
62 introducing a substantial aerosol load into the atmosphere. NPF has been observed in different
63 environments, including pristine (Asmi et al., 2016; Jang et al., 2019; Jokinen et al., 2018), polluted
64 boundary layers and urban areas (Kulmala et al., 2021; Kulmala et al., 2017; Manninen et al., 2010;
65 Kulmala et al., 2016; Wang et al., 2017; Cai and Jiang, 2017; Deng et al., 2020; Yao et al., 2018; Du
66 et al., 2021; Yan et al., 2021), boreal forests (Buenrostro Mazon et al., 2016; Dada et al., 2017;
67 Kulmala et al., 2013; Kyrö et al., 2014; Leino et al., 2016; Nieminen et al., 2014; Rose et al., 2018),
68 tropical forests (Artaxo et al., 2013; Wimmer et al., 2018) and mountain tops (Bianchi et al., 2016,
69 2020). Few studies have investigated NPF processes in a coastal environment although the coastal
70 NPF research started quite early. The investigation of coastal aerosol events dates back to 1978, when
71 the measurements of total aerosol number concentration were carried out at the Tasmanian coast
72 (Bigg and Turvey, 1978). After that atmospheric nucleation was observed in the Southern hemisphere
73 around the Antarctic coastline (O'Dowd et al., 1997), in Mace Head (Flanagan et al., 2005; McFiggans
74 et al., 2004; O'Dowd et al., 2002), in coastal regions of China and Spain (Yu et al., 2019; Mc Figgans
75 et al., 2010; Mahajan et al., 2011) and in open water regions of North East Greenland (Dall'Osto et
76 al., 2018). Most of these studies have identified biogenic emissions from marine algae as the main
77 precursors driving the new particle formation.



78 It is well documented that sulfuric acid (henceforth SA) is an important precursor to
79 NPF in most environments (Almeida et al., 2013; Kulmala et al., 2013; Croft et al., 2016; Jokinen et
80 al., 2017; Kirkby et al., 2011; Sipilä et al., 2010). The advancement in aerosol research, revealed that
81 a binary system of SA and water is not sufficient to produce particles in ambient atmospheric
82 conditions without stabilizing compounds (Benson et al., 2008; Duplissy et al., 2016; Kirkby et al.,
83 2011). More recently, it has been found that a ternary system involving SA-ammonia-water or SA-
84 amines-water yield much higher nucleation rates as compared to the binary system (Kulmala et al.,
85 2000; Benson et al., 2008; Almeida et al., 2013; Glasoe et al., 2015; Kürten et al., 2016). In addition
86 to these systems, organic compounds which are highly oxygenated - thus less volatile- have been
87 found to contribute to secondary organic aerosol (SOA) mass in forested areas, mountain tops and
88 anthropogenically influenced field sites (Ehn et al., 2014; Pierce et al., 2011; Riipinen et al., 2012;
89 Zhang et al., 2009; Heikkinen et al. 2020; et al., 2020) and laboratory experiments have shown that
90 they can contribute also to the first steps of NPF (Simon et al., 2020; Lehtipalo et al., 2018; Kirkby
91 et al., 2016; Tröstl et al., 2016) .

92 Furthermore, another important molecular class, iodine as well as its related oxidized
93 species play a crucial role in NPF especially in coastal areas (Allan et al., 2015; Mahajan et al., 2009;
94 Raso et al., 2017; Sipilä et al., 2016) and in pristine marine locations (Baccarini et al., 2020; Beck et
95 al., 2021; He et al., 2021). Some previous studies have reported the emissions of I₂ from the
96 macroalgae at coastal sites (Huang et al., 2010; Peters et al., 2005; Saiz-Lopez and Plane, 2004).
97 Several studies from coastal sites like Roscoff, France (Mahajan et al., 2009; McFiggans et al., 2010),
98 Mace Head, Ireland (O'Dowd et al., 2002) and other European coastlines (Mahajan et al., 2011; Saiz-
99 Lopez et al., 2012) have reported iodine species initiating NPF. The reported events can be considered
100 as aerosol burst events with high aerosol concentration and having exceptionally high initial growth
101 rates (GR) (O'Dowd et al., 2002; McFiggans et al., 2004; Mahajan, et al., 2011). The study from the
102 Roscoff coast suggests that the daytime emissions of I₂ (produced by macroalgae) during low tides
103 drives the particle formation (McFiggans et al., 2010). The iodine oxides and/or oxoacids formed by
104 the biogenic emissions from the micro- and macroalgae near the coastal regions are capable of self-
105 clustering, which could form new particles with a diameter <3 nm and sometimes with a high gas
106 concentration reaching up to 10⁶ cm⁻³ or even more. Recent studies have shown that ion-induced iodic
107 acid nucleation proceeds at the kinetic limit and the overall nucleation rates (ion-induced nucleation
108 + neutral nucleation) driven by iodine oxoacids (iodic acid, HIO₃ and iodous acid, HIO₂) are high,
109 even exceeding the rates of well-known precursors of NPF (He et al., 2021b, 2021a): sulfuric acid
110 with roughly 100 pptv ammonia under similar conditions (Sipilä et al., 2010). The rapid photolysis
111 of I₂, (< 10 s), produces I atoms above the ocean surface and can be detected in high concentrations



112 close to the source region (McFiggans et al., 2010). However, the compounds with longer lifetimes
113 such as CH₃I (two days) provide a source of iodine throughout the troposphere (Saiz-Lopez et al.
114 2012).

115 Another important gaseous precursor of NPF, SA, could have different sources in
116 Helsinki (Dada et al., 2020b; Väkevä et al., 2000). Dimethyl sulfide (DMS) oxidation by OH radical
117 in the daytime and by nitrate radical in the nighttime yields other aerosol precursor gases, such as
118 methane sulfonic acid (henceforth, MSA) and SA (Barnes et al., 2006), which play a crucial role in
119 the NPF processes. In a marine coastal environment, MSA concentrations, which are typically lower
120 than those of SA, could be as low as 10% of SA concentration and could maximally reach 100% of
121 SA concentration (Eisele and Tanner, 1993), yet MSA is a potential candidate to participate in the
122 atmospheric nucleation and growth processes (Beck et al., 2021). The stability of heterogeneous
123 MSA clusters have been studied in laboratory and modelling studies (Chen et al., 2020, 2015, 2016)
124 but no study has yet documented MSA clusters in the field. The limited NPF studies in the coastal
125 regions and the dynamic coastal atmospheric chemistry drives the motivation of this research. No
126 detailed studies of NPF events were done before taking into account biogenic precursor gases near
127 the coast of Finland despite the fact that extensive cyanobacteria blooms occur every year in the Baltic
128 Sea region and neighboring water bodies (including Finnish lakes) (Kahru and Elmgren 2014), which
129 could be a significant source of iodine species, SA and MSA. In addition, there is a lack of studies
130 reporting the MSA concentrations in the atmosphere of Finland. Thus, this study was undertaken to
131 understand particle formation processes, when the air plume is a mixture of anthropogenic as well as
132 biogenic gases and particles as in the coastal semi-urban location in Helsinki, Finland.

133 Investigating the origin and chemistry of NPF events in an urban coastal setting could be quite
134 challenging since precursor vapors of nucleation are likely a mixture of both anthropogenic and
135 biogenic vapors from different sources. Further, pre-existing particles in the atmosphere affect the
136 occurrence of NPF events by acting as sink for precursor gases and freshly formed particles
137 preventing the latter from further growth. These parameters, in turn, are influenced by the local
138 meteorological parameters such as wind direction, wind speed, (air mass) turbulences especially at
139 the surface layer of the lower atmosphere. Coastal locations are dynamic environments with rapid
140 changes in meteorological parameters, also making the study of NPF more challenging. The
141 meteorological condition could likely govern the removal of particles from the air stream preventing
142 the growth of newly formed particles.

143 In this study, we aim at a thorough evaluation of aerosol precursor molecules with a
144 detailed (NPF events) analysis during the cyanobacterial bloom period, in the coastal-city of Helsinki,



145 Finland, from June to August (summer) 2019. This work evaluates the role of phytoplankton blooms
146 and meteorological parameters in the NPF events observed during the measurement period. We also
147 identify the major precursor vapor(s) and molecular clusters found during the aerosol events. Here,
148 we formulate the hypothesis that gaseous precursors formed from the biogenic emissions from the
149 surrounding marine areas could play an important role in the nucleation processes in Helsinki.
150 Although Helsinki is a coastal area yet the role of marine emissions on New Particle Formation
151 processes has not been studied before.

152

153 **2 Measurement Site and Methodology**

154 To understand the chemical composition of the precursor vapors emitted from various sources
155 around the site, the Chemical ionization Atmospheric Pressure interface-Time Of Flight mass
156 spectrometer (CI-APi-TOF) was operated from the 4th floor laboratory of the Physicum building,
157 Kumpula campus, University of Helsinki (60° 12' N, 24° 58' E ; 49m , a.m.sl). The other aerosol and
158 trace gases instruments were operated at the SMEAR III station which is 180 m away from the mass
159 spectrometric measurement site (Station for Measuring Ecosystem-Atmosphere Relation (SMEAR
160 III), 60.20° N, 24.96° E; 25 m a.s.l.).

161 The measurement sites are surrounded by coastal water bodies (<4km,
162 Vanhankaupunginselkä), forests (<3km) and road connecting to the main city (<300m) as seen in
163 figure 1. Overall Helsinki is located on a relatively flat land on the coast of the Gulf of Finland. The
164 Helsinki Metropolitan area is about 765 km² with approximately one million inhabitants, counting
165 together the city of Helsinki and the neighboring cities of Espoo, Vantaa, and Kauniainen. The climate
166 in southern Finland can be classified as either marine or continental depending on the air-flows and
167 pressure systems. Either way, the weather is milder than typically at the same latitude (60°N) mainly
168 due to the Atlantic Ocean and the warm Gulf Stream.

169 The site and measurement period (25 June 2019–18 August 2019) selected for this
170 particular study are unique. We hypothesize that the biogenic emissions from summertime
171 cyanobacterial blooms in the Baltic Sea and the neighboring water bodies could influence the new
172 particle formation processes at this semi-urban location. The blooms in the Baltic Sea region are
173 recurring phenomena during the summer. Increasing temperatures and the excessive nutrient load in
174 the Baltic Sea promote algal growth (Kuosa et al., 2017; Suikkanen et al., 2007, 2013). According to
175 HELCOM (Baltic Marine Environment Protection Commission), the Baltic Sea has warmed 0.3° C
176 per decade, however after 1990 significantly faster at 0.6° C per decade and in Finnish coastal areas
177 the warming is even faster with a 2° C increase since 1990 (Humborg et al. 2019). The amount of
178 blue-green algae (i.e. cyanobacteria) has shown a statistically significant increase in open sea areas



179 in the Gulf of Finland, Sea of Åland and the Sea of Bothnia in the last 40 years (Kahru and Elmgren,
180 2014). Although nutrient pollution has showed a decreasing trend (Andersen et al., 2017), growing
181 oxygen deficient waters recirculate nutrients and perpetuate cyanobacterial blooms (Funkey et al.,
182 2014). The increase in frequency and intensity of cyanobacterial blooms would increase the potential
183 emission of biogenic gases changing the composition of the overlying atmosphere and the atmosphere
184 of the neighboring sites, depending on the meteorological conditions.

185

186 **2.1 Main Instruments**

187 The Atmospheric Pressure interface-Time Of Flight (APi-TOF) mass spectrometer is
188 the state-of-the-art instrument for gas phase chemical composition investigations including aerosol
189 precursor characterizations. Here the instrument is coupled with a chemical ionization (CI) inlet in
190 order to measure neutral gas-phase molecules that are clustered and charged with a reagent ion. The
191 Time Of Flight (TOF) mass analyzer can detect molecules with masses up to 2000 Th with a mass
192 resolution of 3600 Th/Th. More details on the working principle of the instrument and calibrations
193 can be found in earlier studies (Junninen et al., 2010, Jokinen et al., 2012; Kürten et al., 2014). The
194 sampled air was drawn in through a 1 m-long, “ $\frac{3}{4}$ ” diameter stainless steel tube with an average flow
195 rate of 10 lpm. In this study, the chemical ionization was done via nitrate ions (NO_3^-) through X-ray
196 exposure of nitric acid (HNO_3 , flow rate: 3 mlpm), saturating the sheath air flow entering the CI (flow
197 rate: 30 lpm), the inlet flow of 10 lpm was reached by using a 40 lpm total flow. The instrument was
198 calibrated prior to the experiment according to (Kürten et al., 2012) resulting in a calibration factor
199 of 1.45×10^9 molecule per normalized unit signal including the diffusion losses in the inlet line. The
200 resulting data (i.e. obtained signals) were averaged to 60 min before the mass calibration step
201 performed through the MATLAB based program tofTools (Junninen et al., 2010). The final
202 concentration of the gases were derived using the equation mentioned in Jokinen et al., 2012.
203 Uncertainties of absolute concentration measured by CI-APi-TOF are estimated to be in the order of
204 $\pm 50\%$, while the uncertainties of relative changes in the concentration are smaller than 10% (Ehn et
205 al., 2014). SA, MSA, IA concentrations and normalized signals of specific HOMs (all figures
206 presented in SI) found in the study are calculated using high resolution peak fitting data. Please note
207 that all HOM sum (monomers and dimers) concentrations were calculated from the Unit Mass
208 Resolution (UMR) data. The

209 Neutral cluster and Air Ion spectrometer (NAIS, Airel Ltd., Estonia, Manninen et al.,
210 2010; Mirme and Mirme, 2013) was used to measure the number size distribution of both positive
211 and negative ions between 0.8 nm and 42.0 nm (electric mobility diameter). The NAIS also measures



212 the number size distribution of total particles (neutral and naturally charged) between 2.5–42.0 nm.
213 It uses two identical differential mobility analyzers (DMA, (Knutson and Whitby, 1975)) for
214 simultaneous measurement of positive and negative ions. The flow rate of the instrument is 60 lpm
215 which is split into 30 lpm for each DMA. The instrument was installed in the SMEAR III station. The
216 data was recorded every 2 s.

217 Larger particles of 6–820 nm were measured using a twin differential mobility particle
218 sizer (DMPS) (Aalto et al., 2001). The instrument was installed in the SMEAR III station. The time
219 resolution of data is 10 minutes.

220 The size distribution of 1–3 nm particles was measured by a Particle Size Magnifier
221 (PSM, Airmodus Ltd., Finland; Vanhanen et al., 2011) in series with a condensation particle counter
222 (Airmodus Ltd., Finland). The PSM was operated by scanning the flow 0.1–1.3 lpm (continuously
223 changing the saturator flow rate) which allows determining the 1–3 nm particle concentration and
224 calculation of particle size distribution. The data was recorded for each second and the duration of
225 each scan was fixed to 240 s. The raw data inversion was carried out through the kernel method
226 (Chan et al., 2020; Lehtipalo et al., 2014). The raw data of the PSM employed a pretreatment filter
227 that calculates the correlation between the observed particle concentration and the saturator flow rate
228 of a single scan and discards scans with significant non-correlation or negative correlation (Chan et
229 al., 2020).

230

231 **2.2 Back trajectory calculations**

232 Back trajectories of the different NPF event days were calculated using the data from the Global data
233 Assimilation System (GDAS) as input into the NOAA Hybrid Single-Particle Lagrangian Integrated
234 Trajectory (HYSPLIT) model (<http://www.arl.noaa.gov/ready/>, Rolph et al., 2017; Stein et al., 2015).
235 We used the isentropic trajectories as they incorporate vertical transport components. The 24 h back
236 trajectories were calculated at an arrival height of 100 m a.g.l. The new trajectory starts every 6 hours.
237 The frequency (%) of trajectory was calculated with the following equation (Eq. (1)).

238

$$\text{Traj. Freq.} = \frac{100 \times \text{number of trajectories passing through each grid square}}{\text{number of trajectories}} \quad (1)$$

239 The trajectory analysis was also performed using the Lagrangian particle dispersion model Flexpart
240 v10.4 (Pisso et al., 2019; Stohl et al., 2005) mainly to assess the residence times of the air masses.
241 Flexpart is a stochastic model used to compute trajectories of hypothetical particles, based on mean
242 as well as turbulent and diffusive flow (Pisso et al., 2019). We have used Flexpart along with ECMWF
243 ERA-Interim wind-fields which has a spatial resolution of $1^\circ \times 1^\circ$ at three hour temporal resolution



244 (Pisso et al., 2019). Flexpart was used to simulate 3-day backward trajectories starting from the
245 particle release point located at SMEAR III (24.5° E, 60.1° N) for the event days. The residence times
246 were normalized for clarity in the all the figures and is shown on a scale of 0 to 1 (Results are included
247 in the supplementary information).

248

249 **2.3 Meteorological and other supporting data**

250 The meteorological data such as wind speed, wind direction, temperature, pressure, relative humidity
251 and other supporting datasets e.g chlorophyll (Chl-*a*), SO₂, O₃ concentration and sea level information
252 was additionally used to interpret the NPF events and support the observations of this work (See table
253 S1 for details). The Chl-*a* satellite images were mapped through the GlobColour level-3. The
254 GlobColour level-3 mapped products present merged data from SeaWiFS, MERIS, MODIS AQUA,
255 VIIRS (O'Reily et al., 2000) sensors to provide robust and high coverage data for Chl-*a*
256 measurements. The merging processes are described in Mangin, 2017. In this study, weighted average
257 method (AVW) for retrieving daily Chl-*a* concentration (mg m⁻³) for latitude: 45 °N to 80 °N and
258 longitude: 20 °W to 60 °E was used. The GlobColour level-3 binned products have a resolution of
259 1/24° at the equator (i.e. around 4.63 km) for global products (Mangin, 2017).The details of these
260 additional supporting data given in SI (Table S1).

261

262 **2.4 Formation and growth rate calculations**

263 The growth rates (GR) were calculated based on the 50% appearance time method using the NAIS
264 ion data from both polarities, depending on the better quality polarity (Dada et al., 2020a; Dal Maso
265 et al., 2016; Lehtipalo et al., 2014). This method uses particle number concentration at different size
266 bins (*D_p*), which are recorded as a function of time. The “appearance time” of particles of size *D_p* is
267 the time when their number concentration reaches 50% of its maximum value during the NPF event.
268 To estimate the maximum GR (kinetic) that can be explained by the condensation of certain vapors,
269 two parametrization methods were used, first by Nieminen et al., 2010 for IA and MSA and the
270 second by Stolzenburg et al., 2020 for SA. The growth estimation from SA condensation recently
271 provided by Stolzenburg et al., 2020 also takes into account the hydration of SA particles and dipole-
272 dipole enhancement which is responsible for increasing the collision rate between neutral molecules
273 and neutral particles. As these parameters were not known for IA and MSA, we used the method by
274 Nieminen et al. (2010) for them. The growth due to MSA could be slightly overestimation by this
275 method (Beck et al., 2021) since the parameterization is based on the assumption of irreversible
276 condensation, but MSA rapidly partitions between gas and particle phases if suitable meteorological



277 conditions prevail. The calculated kinetic GR was compared with the total measured particle GR to
278 determine the contribution of each vapor to the growth process (discussed in further sections).

279 The formation rate of the total particles of diameter 1.5 nm is calculated using the time
280 derivative of the particle number concentration measured using the PSM in the size range 1.5–3 nm.
281 The formation rate was corrected for the coagulation losses and growth out of the bin following the
282 method explained by Kulmala et al. 2012. The formation rate of the charged particles was calculated
283 from the time derivative of ions measured using the NAIS in ion mode in size range 1.5–3 nm from
284 both polarities. The formation rate of ions was corrected for coagulation sink, growth outside of the
285 bin, ion-ion recombination and ion-neutral attachment as previously discussed in Kulmala et al. 2012.
286

287 **2.5 Condensation sink**

288 The condensation sink (CS) plays an important role in understanding aerosol dynamics. This
289 parameter determines how fast gas molecules will condense on the pre-existing particles (Dal Maso
290 et al., 2002; Kulmala et al., 2005, 2012). In this study, CS has been calculated by using the DMPS
291 data, according to Pirjola et al., 1999.

292

293 **3. Results and discussions**

294 **3.1 Meteorological parameters and cyanobacterial bloom during the study.**

295 **3.1.1 Meteorological Parameters**

296 The meteorological parameters, especially the wind speed, wind direction and ambient temperature,
297 varied significantly during the study period. The time format in the entire study is UTC+02:00 h. This
298 study period includes the hottest summer days of Finland in year 2019. The average temperature
299 during 17–28 July (the warmest period) was 21.6° C with a maximum temperature of 31.6° C recorded
300 on the 28 July (Fig. 2). Temperature starts to decrease after 29 July. The average temperature in
301 August was 16.5° C with a maximum temperature of 21.9° C recorded on 5 August 2019.

302 The wind direction was highly variable during June–July period. The wind direction in
303 July was mostly from the sectors 270°–320° (West-Northwest) and 90°–150° (East-South East). In
304 August, the wind gained more stability and was dominantly blowing from 180°–270° (South-West)
305 (Fig. 2). The wind speed also showed high variability in June–July. The wind speeds during June and
306 early weeks of July were mostly >6.5 m s⁻¹, followed by a bit calmer mid-July (mostly <=4 m s⁻¹)
307 with preceding high winds in end of July until mid-August (gusts of winds > 5.2 m s⁻¹) (Fig. 2).
308 However, the average wind speeds in both the months was 3 m s⁻¹. The average daylight hours in July
309 were 17–18 hours with the daytime hours between 04:00–22:00 h which starts to decrease in August
310 to 15–16 hours of daylight per day (05:00 h – 21:00 h) as per the Global radiation data obtained from



311 SMEAR III station for the study period. Therefore, the actual nighttime hours in our measurement
312 site can be considered from 23:00 h–03:00 h during Finnish summers.

313

314 **3.1.2 Cyanobacterial bloom conditions during the study**

315 The Baltic Sea (defined from 53° N to 66° N latitude and from 10° E to 30° E longitude inclusive of
316 Gulf of Bothnia, Gulf of Finland and Gulf of Riga) is characterized by usually two algal blooms
317 occurring in early Spring (mostly diatoms) and a Summer bloom increasingly dominated by
318 cyanobacteria (blue green algae). The summer bloom period selected for this study was typically
319 characterized by cyanobacteria. When these microscopic cyanobacteria multiply and aggregate, they
320 are seen as blue-green patches or scum-like layers over the surface of lakes and marine waters. The
321 warm early summer temperatures (during June) resulted in a cyanobacterial bloom (Finnish national
322 monitoring; SYKE, 2019). However, the weather conditions in July began changing with high winds
323 causing the cyanobacteria to be highly mixed in the water column, which reduced bloom intensity at
324 the sea surface to lower than normal in July and August. Subsequently, temperatures were lower in
325 August as compared to July and windier as compared to other summer months. These windy
326 conditions kept the lake cyanobacteria well mixed in the water. The northern Baltic Sea, including
327 the Gulf of Finland, the Southern parts of the Åland islands and even the Bothnian Sea occasionally
328 observed massive blooms of cyanobacteria during June–August 2019. However, the bloom intensity
329 of cyanobacteria at the coastal areas were intermittent and changed rapidly due to the spatial
330 complexity of the coastline and variable winds and currents.

331 These cyanobacterial blooms are generally dominated by three taxa, *Nodularia*
332 *spumigena*, *Aphanizomenon* sp. and *Dolichospermum* sp. (Knutson et al., 2016; Kownacka et al.,
333 2020). In the Baltic Sea, these cyanobacteria actually contribute the most to the total pelagic nitrogen
334 fixation (Klawonn et al., 2016). Other potential primary producers emitting vapors are the littoral
335 macroalgae growing along the shallow coastline. For example, the perennial macroalgae, *Fucus*
336 *vesiculosus* covers large areas of the coastal areas of Baltic Sea, where they support very high biomass
337 and high productivity (Attard et al., 2019). Low sea levels (0.2–0.8 m) were recorded in mid-July (11
338 July 2019–27 July 2019) during the period when high temperatures (20° C and above) prevailed
339 (Fig.2) in our study region. During these conditions, contributors to emissions might be a mix of both
340 coastal macroalgae and open sea microalgae. There is a possibility that reasonably, large extents of
341 coastal macroalgae, including *F. vesiculosus*, were exposed to direct sunlight (in shallow waters or
342 low tide conditions) hence making this time window favorable for observing potentially high
343 emissions in gas phase from macroalgae, in addition to the emissions from cyanobacterial blooms.
344 However, in the semi-urban/coastal setting of this measurement site, there could be various other



345 parameters, which also could play a role in determining the concentrations of the biogenic emissions;
346 for example the wind speed and wind direction. The atmosphere in this semi-urban coastal location
347 is itself a cocktail of various vapors, oxidants and particles, which would affect the quantification,
348 source apportionment and characterization of the biogenic emissions.

349

350 **3.2 Precursor vapor concentrations and their sources**

351 The measured daytime precursor vapor concentrations showed a regular diurnal cycle consistent with
352 the photochemical production of SA and IA in 90% of the days in this study. SA, key precursor of
353 atmospheric NPF, is formed mainly by reaction of sulphur dioxide with OH-radicals, which is
354 predominantly controlled by the photochemical cycles (e.g. Sipilä et al., 2010; Jokinen et al., 2017).
355 The mean (whole day) concentration of SA in July and August was 2.98×10^6 molec. cm^{-3} and 2.67
356 $\times 10^6$ molec. cm^{-3} respectively. The mean concentration is slightly lower than compared to the
357 concentrations of SA reported by very recent study measured in a Helsinki street canyon, 1×10^7
358 molec. cm^{-3} (Olin et al., 2020) but similar to the SA concentration measured at the SMEAR III station
359 in 2018 (Okuljar et al., 2021). In the study of Olin et al., 2020, SA concentrations were greatly
360 affected by vehicular traffic as the site is situated at a busy street canyon. The SMEAR III is
361 considered as a background site much less affected by vehicular traffic (Okuljar et al., 2021). In
362 comparison to other locations, the daytime SA concentration in pristine Antarctic region has been
363 reported from 10^5 up to 10^7 molec. cm^{-3} (Mauldin et al., 2001, Jokinen et al., 2018), 10^6 molec. cm^{-3}
364 in remote continental, remote marine and forest regions and 10^7 molec. cm^{-3} in urban and rural
365 agricultural lands using the same technique as in here (Berresheim et al., 2000; Kuang et al., 2008;
366 Petäjä et al., 2009; Kurtén et al., 2011; Zheng et al., 2011; Chen et al., 2012; Jokinen et al., 2012;
367 2017, Kürten et al., 2014; Bianchi et al., 2016; Baalbaki et al., 2021; Dada et al., 2020b). It has been
368 well documented that SA contributes to aerosol formation and growth processes (Boy et al., 2008;
369 Eisele et al., 2006; Fiedler et al., 2005; Iida et al., 2008; Sarnela et al., 2015; Jokinen et al., 2018;
370 Kürten et al., 2015, 2016; Mauldin et al., 2001; Paasonen et al., 2010; Wang et al., 2011; Weber et
371 al., 1998, 1999; Yao et al., 2018; Dada et al., 2020b). Most of these studies are conclusive that SA
372 concentration in the atmosphere depends on the anthropogenic and biogenic activities around the site.

373 In the coastal marine boundary layer, the MSA concentration is typically 10–100% of
374 that of SA (Berresheim et al., 2002; Eisele and Tanner, 1993). Until recently, no studies have been
375 found to report MSA and IA concentrations in coastal/urban setting of Finland. The mean (whole
376 day) concentration of MSA in July and August was almost similar, 4×10^5 molec. cm^{-3} . The mean
377 concentration of IA in July and August was 1.27×10^6 molec. cm^{-3} and 2.69×10^6 molec. cm^{-3} ,
378 respectively, showing two times increase in IA concentrations in August (Fig. S1). A similar increase



379 in IA concentrations from summer to autumn were observed in the Arctic Ocean, where the increase
380 in IA was attributed to the freezing onset of the pack ice and increase in ozone concentrations
381 (Baccarini et al., 2020). However, here the increase is mainly due to the change in the air mass arriving
382 at the experimental site, enriched with biogenic emissions from the blooms. For the same period, the
383 CI-API-TOF data shows exceptionally high concentrations of highly oxygenated organic molecules
384 (HOMs), with monomer concentrations (300–450 amu) of 10^8 molec. cm^{-3} and HOM dimer
385 concentrations (450–600 amu) of 10^8 molec. cm^{-3} as well (Fig.S2).

386 In more details, the IA concentration rises one order of magnitude, from 10^6 to 10^7
387 during the 11–17 August, when the wind direction changes abruptly (from 280° – 360° to 180° – 230° ,
388 marine air mass, Fig. 3). We found that during the marine air (180° – 230° , South Easterly, over Gulf
389 of Finland and South westerly, over Northern Baltic sea) influence over the study region the average
390 noontime maximum of SA, IA is on the order of 10^7 molec. cm^{-3} and MSA is around 10^6 molec. cm^{-3}
391 (Fig. 3). This is one order of magnitude higher concentration than when the wind was from over
392 land (Fig. 3).

393 The highest concentration, 3.2×10^7 molec. cm^{-3} of IA was observed when the wind is
394 coming from the Baltic sea sector, whereas the highest SA concentrations ($\sim 3.0 \times 10^7$ molec. cm^{-3})
395 we observe when air mass travelled over the countries of Estonia and Russia crossing Gulf of Finland
396 before entering the measurement site (land+sea region). The connection between the aerosol
397 precursors and the wind direction can be observed in the cases where the wind direction changes
398 rapidly. The highest IA concentration was recorded when the wind direction changes after the 4
399 August, 180° – 230° (the Baltic Sea region). The change in wind direction was clearly reflected in a
400 reversal of the concentration trends of SA and IA (Fig. 3). It was observed that the winds coming
401 from 80° – 180° or 250° – 280° (land-sea region, Fig. 3) were SA rich air masses. This comprises of the
402 landmasses of south and northeastern Finland, Northern Russia, part of Gulf of Finland and Estonia
403 and North-North western part of Finland including a part of northernmost Gulf of Bothnia. The sector
404 0° – 90° or 280° – 360° (land, Fig. 3) consists mostly of urban cities.

405 During the entire study period, when the air plume passed over the northern Baltic Sea region and
406 the wind speed was high enough ($> 4 \text{ m s}^{-1}$) high concentrations of IA was observed. While IA can be
407 exclusively sourced from the marine and biogenic emissions (Mahajan et al., 2011; O’Dowd et al.,
408 2002; Sipilä et al., 2016; Carpenter et al., 2021), SA could be biogenic or /and anthropogenic. Further,
409 the temperatures prevailing during this period may have facilitated the DMS oxidation at a higher
410 rate, which forms the source of biogenic SA and MSA. However, this is not a very simple equation,
411 since this fractional yield of (biogenic) SA from DMS oxidation additionally also depends on the
412 atmospheric NO_x ($\text{NO} + \text{NO}_2$) and HO_x ($\text{OH} + \text{HO}_2$) levels and on the scavenging of SO_2 by sea salt



413 or cloud droplets (Hoffmann et al., 2016). The anthropogenic sources of SA for this site includes
414 vehicular or ship traffic especially considering that there is a city road just 250 m and a harbor 6 km
415 away from the measurement site. We explored the correlations of SA to a biogenic proxy, MSA and
416 correlation with NO_x (anthropogenic proxy) to have a clear source apportionment of SA (Fig.4). SO_2
417 could not be treated entirely as anthropogenic proxy as it can be sourced from DMS oxidation as well.

418 The good correlations ($r_s > 0.6$, Fig. 4a and 4b) between SA and MSA during the study period
419 (June–August) could suggest that they were sourced from a common biogenic source, the DMS
420 emission from the cyanobacterial bloom. Good correlations of SA and MSA was also found in August
421 ($r_s = 0.8$, Fig.4b) when the air mass was mostly marine (and/or from the Finnish coastline, Fig. 3).
422 Another observation was that SO_2 also shows some correlations with SA in both June-July and August
423 study periods ($r_s = 0.4$, Fig. 4c and 4d), but not as significant as SA and MSA correlations. SO_2 can
424 have different sources unlike MSA which is mostly biogenic, hence these observations could possibly
425 indicate SA was more biogenic than from other sources. But we cannot be very accurate in this
426 estimation only by analyzing the correlation coefficients since both MSA and SA can have a similar
427 daily cycles due to the oxidation pathways.

428 Both SO_2 and MSA are the oxidation products of DMS (produced by phytoplanktons, including
429 some cyanobacteria), oxidized through OH and NO_3 radical (Chen et al., 2000). Some of the previous
430 chamber studies have confirmed that SO_2 is the major intermediate products formed from DMS
431 oxidation (Sørensen et al., 1996; Berresheim et al., 1995). The SO_2 could be oxidized to SA (OH/ O_2
432 oxidation) during the transport. Since our experimental site was surrounded by water bodies and the
433 summer season had enriched most of these freshwater and marine waters with abundant
434 cyanobacterial blooms, this biogenic SA contribution to the study site has to be accounted when
435 analyzing the sources of SA. However, SO_2 can also be sourced from various anthropogenic activities
436 and can be oxidized to SA. In Finland the major sources of anthropogenic SO_2 is the public power
437 industries contributing to almost 90% to the total SO_2 emissions in Finland in the year 2019, while
438 transport contributing to less than 1% according to the emission inventory prepared by Finnish
439 Environment Institute, SYKE (Finnish Air Pollution Inventory; [ymparisto.fi/en-](https://ymparisto.fi/en-US/Maps_and_statistics/Air_pollutant_emissions)
440 [US/Maps_and_statistics/Air_pollutant_emissions](https://ymparisto.fi/en-US/Maps_and_statistics/Air_pollutant_emissions)). Further the maximum data points of high
441 concentrations of SO_2 ($\sim 10^7$ molec. cm^{-3}) were not observed during the traffic hours in June-July-
442 August (Fig. 4c and 4d) another possible indication that biogenic sources could be contributing to the
443 SO_2 concentrations and thus SA concentrations near the study site.

444 The emission inventory of Finland for the year 2019 indicated that sources of NO_x as NO_2 were
445 mainly the power industries (41.5%) and the transport sources (41%) ([ymparisto.fi/en-](https://ymparisto.fi/en-US/Maps_and_statistics/Air_pollutant_emissions)
446 [US/Maps_and_statistics/Air_pollutant_emissions](https://ymparisto.fi/en-US/Maps_and_statistics/Air_pollutant_emissions)). These sources are indeed the most significant



447 sources of NO_x globally (Meixner and Yang, 2006) NO_x , definitive proxy of anthropogenic influence
448 shows a poor correlation with SA ($r_s=0.28$, Fig. 4e) during June-July also suggest insignificant effect
449 of traffic on the SA concentrations. Unfortunately, the NO_x data from August was unavailable due to
450 instrument malfunction.

451 After carefully analyzing the data presented in Figure 3, where we observe high SA concentrations
452 even when the air mass was marine and the good correlations of SA-MSA (inclusive of insignificant
453 correlations of SA- NO_x) (Fig. 4) indicate towards a greater possibility of the influence of biogenic
454 emissions on the concentrations of SA as compared to the anthropogenic emissions.

455

456 3.3 Types of nucleation events during the study

457 During, 25 June 2019–19 August 2019, we observe a number of NPF events characterized by a short
458 appearance of ultrafine particles in the number size distribution lasting for less than one hour. These
459 so-called bursts /spikes appearing at small sizes (sub-3 nm) are indicative of local clustering and NPF
460 processes in contrast to regional events, where it is possible to follow the growing particle mode for
461 several hours (Dada et al., 2018; Dal Maso et al., 2005). We do observe transported events (events
462 with a growing particle mode, but no small particles forming at the site) and non-events days but they
463 are not included in the analysis. This section discusses the occurrence of local and regional new
464 particle formation events with the focus on: 1) trace gases variability during the event days, 2) the
465 evolution of different sized particles during these events, 3) the impact of meteorological parameters
466 and 4) the effect of cyanobacterial bloom on the events.

467 3.3.1 Nucleation: Regional and Local events

468 A regional NPF event was observed on 30 June 2019, which starts at 08:45 h and ends at 13:23 h (Fig
469 5a). The negative ion clusters start to increase in concentration first at 08:45 h (Fig. 5b) concurrent
470 with the increase in concentration of the smallest particles (<3nm) from 10^2 to 10^3 cm^{-3} (Fig. 5c).
471 Subsequently, SA concentration doubles from 2×10^6 to $4 \times 10^6 \text{ molec. cm}^{-3}$ (Fig. 5d), while the particle
472 formation rate at 1.5 nm ($J_{1.5}$) increasing from $0.3 \text{ cm}^{-3} \text{ s}^{-1}$ to $0.6 \text{ cm}^{-3} \text{ s}^{-1}$. $J_{1.5}$ was much higher than
473 either of $J_{1.5}^-$ and $J_{1.5}^+$, thus indicating a neutral formation pathway rather than an ion mediated one.
474 Further we also observe local clustering event at 15:00 h with simultaneous increase of concentration
475 of SA and HOMs along with increase in the smallest particle concentration. This possibly indicates
476 the role of SA and HOMs in the nucleation initiation. The work of Okuljar et al. (2021) also report
477 an increase in sub-3 nm particles with a simultaneous increase in SA concentration at the SMEAR III
478 site, supporting our observations. However, the role of HOMs in nucleation initiation has not been
479 explored at this site.



480 A clear increase in nucleation mode particles is seen during the event, starting at 08:45
481 h (234 cm^{-3}) and reaching its maximum at 12:30 h (4589 cm^{-3}). This increase in concentration of the
482 nucleation mode particles was followed by the increase in concentration of Aitken mode and
483 accumulation mode particles and continues for a couple of hours, indicating growth of particles (Fig.
484 5e), possibly reaching to CCN relevant sizes. The growth continues until the wind direction suddenly
485 changed after 12:00 h (Fig. 5d), that apparently discontinued the precursor vapor source to our site.
486 After the change in local wind direction, the observed SA and IA slightly increase, and we still
487 observe local clustering (formation of small ions and particles), but no continuous growth typical for
488 regional events. Figure 5f shows that >40% of the trajectories passes above the Swedish island of
489 Gotland towards southern part of Bothnian Sea. The MODIS data shows that the bloom was present
490 in the Bothnian Sea, but not quite dense as compared to the southern Baltic Sea (south of Gotland
491 island) and the northern part of the Gulf of Finland. The majority of the trajectories did not pass over
492 the dense cyanobacterial bloom patch during this day (Fig. 5f). The calculated (normalized) residence
493 time was higher over the neighboring cities of Helsinki (Southwestern side) and parts of Bothnian
494 Sea during the event time (see Fig. S3). Thus the land based anthropogenic activities and biogenic
495 sources both can be contributing to SA concentrations for this event; here we cannot exactly quantify
496 the source types for SA. However, the source of SA from the local sources such as vehicular traffic
497 around our measurement site is small (as discussed above) but cannot be completely ignored (Olin et
498 al., 2020).

499 The high signals (normalized) of DMA-SA cluster seen during the entire event (rising
500 from the start of NPF event) indicates SA clusters initiate the event (Fig.S4a). The increase of HOMs
501 is also clearly observed during the event Fig. S4b. Therefore we suggest that nucleation and growth
502 of particles was possibly due to SA-organics which ensures that particles reach the CCN and thus
503 climate relevant diameters.

504 The particle GR (7–25 nm) for this event was 16.5 nm h^{-1} , which is typical of a coastal
505 site. Even when several condensing vapors participate in the growth process, growth rates typically
506 do not exceed 20 nm h^{-1} (Kulmala et al., 2004). The GR for organics was calculated after subtracting
507 the combined contribution of the GR of SA, IA and MSA from the measured particle GR. The GR
508 for organics should be treated as an estimation since no separate GR calculations and assumptions
509 were used. The calculated growth rates (GR) shows that SA can explain maximum 41% of the growth
510 of sub-3 nm particles, while IA and MSA can explain only <1% of the GR in this size range. The GR
511 by SA in the bigger size fraction (7–25 nm) was only 0.51 nm h^{-1} explaining only 3% of the measured
512 growth rate of particles. This means that vapors other than SA, IA and MSA were responsible for
513 96% of the measured particle growth. These other vapors could include different organics since



514 organics are known to contribute to growth of particles (Kulmala et al., 1998, 2004; Riipinen et al.,
515 2012; Zheng et al., 2020) and explain particle growth in the boreal forest (Ehn et al., 2014).

516 Another example of regional event (neutral nucleation) probably driven by SA and organics was
517 observed on 30 July 2019 (Fig. S5) which lasts for around four hours. The trajectory frequency plots
518 showed that most of the trajectories were from the northern land areas (including urban cities and
519 boreal forests) of Finland with highest residence times over these land regions (Fig. S6). Therefore,
520 the precursor gases from the biogenic origin, IA and MSA do not show a significant concentration
521 increase during this event and hence assumed to be contributing insignificantly to this event. The
522 greater residence times over the land areas clearly support the high SA and organic concentrations
523 seen during the event indicating a SA-HOMs driven local event (Fig. S6). In this case, the growth
524 due to SA explains 60% of growth of sub-3nm particles compared to 41% when the dominating
525 trajectories passed over the Gulf of Finland (Fig. 5, 30 June 2019). Still, as for the previous case, a
526 major fraction of the growth in the 3–7 nm range remains unexplained by the available acids (SA, IA,
527 MSA) and is expected to be related to organic material being abundant. The GRs explained by SA
528 in both sub-3 nm (1.93 nm h^{-1}) and 3–7 nm (1.46 nm h^{-1}) size ranges are 58-59% higher than on 30
529 June 2019 (0.79 nm h^{-1} and 0.61 nm h^{-1} for sub-3 nm and 3–7 nm, respectively) which could be
530 explained by the increase in SA by 52% on 30 July 2019. Thus, the events on 30 June and 30 July
531 possibly occur via the nucleation of sulfuric acid (possibly stabilized by bases eg. ammonia or amines)
532 and the HOMs contribute to growth of particles and possibly in nucleation as well.

533

534 3.3.2 Nucleation: Burst events

535 Case 1: Biogenic IA nucleation- burst/spike events, 11 August.2019

536 Intense burst events are frequently observed at coastal sites accompanied with high concentrations of
537 IA (O'Dowd et al., 2002; Rong et al., 2020; Sipilä et al., 2016). Two of such bursts or spike events
538 were observed on 11 August 2019 at 04:00 h and 13:00 h (Fig. 7a). Only the second spike event was
539 observed in the NAIS size distribution with a higher intensity in the negative mode at 13:00 h (Fig.
540 7b). During both these spike events we observe the formation of clusters (1.5 nm) and the formation
541 rate ($J_{1.5}$) increases from 0.2 to $3.7 \text{ cm}^{-3}\text{s}^{-1}$ during the event with a simultaneous significant increase
542 in the sub-3 nm particle concentrations from ~ 100 to $>2000 \text{ cm}^{-3}$ (Fig. 7c). $J_{1.5}^+$ and $J_{1.5}^-$ remain lower
543 than the total formation rate indicating this event to be a case of neutral nucleation. At the same time,
544 IA shows increase in concentration from $9.2 \times 10^5 \text{ molec. cm}^{-3}$ at 03:00 h to $1.2 \times 10^6 \text{ molec. cm}^{-3}$ at
545 04:00 h. During this event the air masses changes from 160° to 140° i.e the direction of the air mass
546 is changed to the Gulf of Finland. In the second burst (at 13:00 h), the IA concentration increases
547 from 2.3×10^6 to $7.3 \times 10^6 \text{ molec. cm}^{-3}$ from 13:00 h to 14:00 h (Fig. 7d) with a slight change in wind



548 direction from 151° to 166° . Most of these air masses are from the Gulf of Finland. SA concentration
549 also increased but remained lower than IA during both the burst/spike events indicating a possibility
550 that iodine oxoacid formation initiates cluster formation (He et al., 2021). We observe a growth of
551 particles until 15:00 h in the particle modes (NAIS data, Fig. 7B). However the particles are seen
552 reaching sizes up to size 100 nm (DMPS data, Fig. 7A). The organics almost remain constant within
553 the range of $2.5\text{--}3.1 \times 10^8$ molec. cm^{-3} . A further increase in IA concentration, 3.18×10^7 molec. cm^{-3}
554 occurs at 15:00 h, and the concentration remains in the range of 10^7 molec. cm^{-3} for another two hours
555 (Fig. 7d). This was the highest observed IA concentration in the entire measurement period. A recent
556 study by He et al., 2021, indicate that HIO_3 concentrations above 1×10^7 molec. cm^{-3} leads to rapid
557 new particle formation at $+10^\circ$ C. At such concentrations the efficacy of iodine oxoacids to form
558 new particles exceeds that of the $\text{H}_2\text{SO}_4\text{-NH}_3$ system at the same acid concentrations. Thus, the
559 concentration of IA found in this event is capable of initiating nucleation, especially since the
560 concentration of IA being two times higher than SA during the start of the event. In addition, a clear
561 increase in the normalized signal of deprotonated IO_3^- with no significant increase in DMA-SA cluster
562 during the event at 13:00 h (Fig. S7a). However, $\text{HNO}_3\text{-IO}_3^-$ cluster was the most abundant followed
563 by the $\text{H}_2\text{O-IO}_3^-$ cluster indicating this event to be IA-driven nucleation. Further, between 14:00–
564 15:00 h, when we observe the highest IA concentrations a subsequent growth of particles is noted.
565 We also observe an increasing number concentration of nucleation mode particles from 13:40 h (~ 650
566 cm^{-3}) to 14:40 h (~ 1800 cm^{-3}). After this one hour of intense clustering, the Aitken mode particles
567 also begin to increase in concentration from ~ 1300 cm^{-3} to ~ 4800 cm^{-3} during 15:00 h–18:00 h (Fig.
568 7E). The total particle concentration increased from ~ 2400 cm^{-3} to ~ 6400 cm^{-3} within an hour during
569 this burst event. We suggest that this burst event was possibly capable of producing particles big
570 enough to act as CCN.

571 The global radiation and brightness parameter suggest that 11 August 2019 was an
572 overall a cloudy day until 12:30 h (Fig. S8). The weather starts to turn into clear-sky after 13:00 h
573 when the brightness parameter increases from <0.3 to ~ 0.7 (Fig. S8). Impact of brightness parameter
574 on NPF is also observed in a previous study (Dada et al. 2017). The clearing of the sky could explain
575 the intense spike at 13:00 h in the particle number size distribution as well as in the acid
576 concentrations. For this particular case, we investigated further the source of such high IA
577 concentrations and we found that during this day, the cyanobacterial bloom was observed in three
578 intense patches in the central Baltic sea, southern Gulf of Finland (ship transect route between
579 Helsinki and Tallinn) and Gulf of Riga (Fig. 7f). The trajectory frequency analysis clearly shows that
580 the maximum frequency of trajectories was observed over southern Gulf of Finland (inclusive of the
581 coastal waters of Suomenlinna island) however we do see the air masses coming in from the central



582 Baltic sea as well which was characterized by intense bloom during this day (Fig. 7f). The sea level
583 was also low as it was observed to be 0.8–0.9 m in the coastal waters in around the measurement site
584 (Suomenlinna and Gulf of Finland coastal measurements sites), supporting the exposure of the macro
585 algae to sunlight which can be a good source of iodine precursors.

586 The residence time of the airmasses coming from the Gulf of Finland and Northern
587 Baltic Sea were longer than the residence time of the airmasses coming from the neighboring land
588 areas (Fig. S9) clearly explaining the source of high IA observed during the event, which is through
589 the blooms. Further, the airmass was completely marine at 15:00 h when the highest IA is recorded
590 supportive of the marine biogenic source of IA and its transport to the measurement site. The distance
591 from the Gulf of Finland to the measurement site is approximately 5–10 km. With the wind speed of
592 5 m s^{-1} recorded during the event, it takes less than one hour for the emission to transfer to our
593 measurement site. By the time the air mass reached our measurement site from the emission source,
594 all of the I_2 was oxidized to IA. However, at this point we cannot differentiate between the sources
595 of IA from neighboring coastal waters and the central Baltic Sea but can speculate that most of the
596 IA observed could be sourced from the nearest coastal locations of Gulf of Finland.

597 Another burst/spike event driven by IA occurred on 14 August 2019 (Fig. S10) when
598 the IA concentration was found to be $8.54 \times 10^6 \text{ molec.cm}^{-3}$ which was 2–3 times higher than SA
599 concentration ($4.2 \times 10^6 \text{ molec.cm}^{-3}$). The event did not last more than 30 minutes. The precursor
600 vapor concentration was not large enough for the event to continue or the particles to grow further.
601 The meteorological conditions were very much similar to this event (11 August 2019). For this event
602 also, the airmass was marine with maximum residence times over the Gulf of Finland and Baltic Sea
603 regions. Vicinity of the emissions to the measurement site enabled the detection of these fast-forming
604 clusters (from the emissions).

605 **Case 2: Biogenic SA nucleation –multiple bursts events**

606 Another kind of event was observed on 15 August 2019 (Fig. 8a) where multiple particle bursts are
607 observed and the particles grow to sizes $> 50 \text{ nm}$.

608

609 The formation rates for the smallest clusters for both the polarities were the same ($J_{1.5^+}$ and $J_{1.5^-}$) (Fig.
610 8b and c). This was also a case of neutral nucleation as inferred from the relatively high (as compared
611 to ions) $J_{1.5}$ (neutrals). On 15 August there was a sudden change of wind direction from the 180° –
612 215° (prominent wind direction during 11–14 August) to 280° and a series of bursts is triggered with
613 the intense formation of clusters ($< 3 \text{ nm}$) at each burst (Fig. 8d). The two most intense burst events
614 (marked as dashed rectangles in Fig. 8a, b, d and e) were associated with an increase in SA from 2.4



615 to 6.43×10^6 molec. cm^{-3} at 06:00 h, and 5.3 to 7.03×10^6 molec. cm^{-3} at 14:00 h (Fig. 8d). A third
616 burst at 09:00 h showed an increase in SA from 3.4 to 6.25×10^6 molec. cm^{-3} at 09:00 h interestingly
617 with IA_{max} : 3.14×10^6 molec. cm^{-3} . In all the three bursts a simultaneous increase in IA and MSA
618 from 03:00 h to 12:00 h is observed, but the SA concentration was two to three times higher than IA
619 and four to five times higher than MSA concentrations. The most intensive burst was at 14:00 h (as
620 compared burst to 6:00 h) when the SA was 3 times higher than IA. This burst was associated with a
621 significant increase in Aitken mode particle concentration (from 1490 at 14:00 h to 4300 cm^{-3} at 15:00
622 h). The increase in accumulation particle concentration was seen just after one hour from the start of
623 the bursts for both events (06:00 h and 14:00 h). However the increase in accumulation mode particle
624 concentration for these two events was not very significant ($\sim 100 \text{ cm}^{-3}$) although particles reaching a
625 size more than 80 nm (CCN relevant sizes) was observed. We saw DMA-SA clusters during the event
626 (Fig. S11) which supports the observation that this a SA-driven NPF event.

627 During both these events (in fact, all the smaller burst events observed during this day), the
628 trajectories were originating from Sweden (24 h prior to arrival). However, before entering the
629 measurement site the trajectories passed over the Southern part of Gulf of Bothnia and the trajectory
630 frequency was $>70\%$ when the wind passed over the cyanobacterial bloom region (Fig. 8f).

631

632 3.4 Possible contributions of biogenic emissions to Precursor gaseous vapors

633 Assuming insignificant anthropogenic SA contribution as discussed in section 3.2, we investigated
634 the other possible sources of SA by evaluating the type of algae present in the water bodies from
635 where the air masses travelled during the events. The marine algae produces
636 dimethylsulfoniopropionate (DMSP), which is capable of forming DMS, which subsequently
637 oxidizes into SA and MSA. While very few cyanobacterial species are capable of producing DMSP
638 (Karsten et al., 1996; Jonkers et al., 1998), and its concentration can vary considerably from one
639 species to another (Keller et al., 1989). Moreover, blooms could be well-mixed with other algal
640 species (ESA report, 2000) which are capable of producing DMSP. A recent experiment identified
641 *Aphanizomenon* as the only cyanobacteria producing DMS (Steinke et al., 2018). The Gulfs of
642 Bothnia and Riga are dominated by the genus *Aphanizomenon* (Kownacka et al., 2020). In addition,
643 the Bothnian Sea and Gulf of Finland were found to be rich in cyanobacterial genera of
644 *Aphanizomenon* along with *Nodularia* and *Dolichospermum* (SYKE 2020).

645 A recent study also indicated that the abundance of DMS producing cyanobacteria,
646 *Aphanizomenon* has increased in the Bothnian Sea due to decreasing salinity (Olofsson et al., 2020).
647 Moreover, marine waters themselves are a large source of DMS (Kettle and Andreae, 2000)



648 explaining the contribution of biogenic SA in the above-mentioned burst events (15 August 2019).
649 Hence to conclude the gulf regions surrounding the experimental site could be potential sources of
650 biogenic SA. Moreover, high iodine emissions could be expected over the Baltic Sea proper region
651 due to the presence of the macroalgal species which are well established and adapted in the Baltic
652 Sea despite its low salinity (Kautsky and Kautsky, 2000; Schagerström et al., 2014) (high IA on 11
653 August 2019 event day). The rocky shorelines of the northern Baltic Sea provide ample habitat for
654 several species of macroalgae, including *F. vesiculosus* (Kautsky & Kautsky 2000, Torn et al., 2006).
655 Previous studies have documented that certain macroalgae contain high levels of iodine (Ar Gall et
656 al., 2004), of which the kelp *Laminaria digitata* stores the highest amount (Ar Gall et al., 2004;
657 Küpper et al., 1998).

658 However recent chamber experiments comparing different species of brown algae
659 found that emission rate of I₂ was higher in the case of *F. vesiculosus* when compared to other species
660 like *L. digitata* (Huang et al., 2013). This could possibly explain the high IA concentration recorded
661 by the CI-API-TOF when the air mass was coming from the Northern Baltic Sea region (11 August
662 2019 and 14 August 2019). High production of macroalgal species is common along the extensive
663 archipelago coastlines of the northern Baltic Sea, and particularly *F. vesiculosus* is likely to contribute
664 with high emission rates, especially when during peak production times when exposed to low sea-
665 levels and direct sunlight. However, partitioning the influence of macroalgae requires further
666 mechanistic studies. We conclude that marine and coastal regions surrounding the measurement site
667 are capable of producing SA and IA during bloom period, which can initiate NPF.

668

669 **4 Conclusions**

670 We studied the composition, concentrations and sources of precursor vapors forming aerosols in
671 Helsinki, Finland during the summer of 2019. The source of precursor gases causing new particle
672 formations were assessed by analyzing the meteorological parameters, situation of cyanobacterial
673 bloom in the Baltic Sea. Our study recorded several regional, local and burst events and we found
674 that they were connected to elevated concentrations of SA and IA. The burst /spike events occurred
675 simultaneously with high intensity cyanobacterial blooms in the Baltic Sea.

676 The study draws the following conclusions. 1) Constantly changing algal conditions in
677 Gulf of Bothnia, Gulf of Finland and Baltic Sea are a significant source for the emission of iodine
678 precursors and DMS. These emission further oxidize in the atmosphere to form IA and SA, which
679 can be detected by mass spectrometric methods. Interestingly, during marine air mass intrusion with
680 higher residence time over the algal blooms, the gaseous precursors formed from the biological
681 emissions possibly exceeded the gaseous precursors sourced from anthropogenic emissions at the



682 measurement site. In fact, an overall higher impact of biogenic emissions was noted in this semi-
683 urban site. 2) Moreover, the meteorological conditions like wind direction (biogenic and
684 anthropogenic source sectors) and wind speed were identified as the most important parameters
685 influencing the precursor vapor concentration reaching the measurement site and thus determining if
686 NPF occurred. These factors will become more important if the measurement site is distant from the
687 coast. Our study infers, that when the air mass travelled over the land with higher residence time of
688 the air mass over the urban areas, it was enriched with SA and organics from proximal-local sources
689 leading to the occurrence of regional and local events (30 June 2019 and 30 July 2019). In contrast,
690 when the air mass travelled over the water bodies, with higher residence times over the cyanobacterial
691 blooms, the air mass was enriched with biogenic IA and/or SA initiating a burst/spike event at the
692 measurement site (11, 14, 15 August 2019). This observation is comparable to other coastal sites like
693 Mace Head, although the NPF events are much stronger in Mace Head, since the measurement site is
694 just at the coast with intensive low tide high tide periods. 3) The formation rates of 1.5 nm particle
695 and ions suggest that both IA-driven and SA-driven NPF events were neutral nucleation events. 4)
696 The type of phytoplankton species, intensity of the bloom and distance of the bloom from the
697 experimental site plays a very important role in determining the concentrations of precursor gases
698 and thus influence the duration and type of NPF. The IA driven nucleation occurred when the air
699 mass travelled from over the Baltic Sea region, where the coasts are dominated by several species of
700 macroalgae, including *F. vesiculosus*. The SA rich burst events occurred when air mass travelled over
701 the Gulf of Bothnia which was mainly dominated by the cyanobacteria species *Aphanizomenon* 5)
702 Burst/spike events, connected to high IA concentrations, likely led to fast growth of particles
703 potentially to CCN sizes. The role of stabilizing the IA clusters by SA and ammonia in a semi-urban
704 coastal place needs to be further explored. The growth rate of particles was not fully explained by the
705 SA, IA and MSA alone, this applies especially for 3–7 nm or larger particles, indicating that organics
706 might be playing a critical role in the growth of particles in this semi-urban location. We have
707 significantly high ambient concentrations of HOMs in this study, although the detailed descriptions
708 is beyond the scope of this work.

709 The role of organics (HOM) in the growth of particles is an active research question.
710 Exploring the sources and characterizing them during a bloom period, when the emission of biogenic
711 volatile organics increase with temperature, is crucial to understand the climate linkages of aerosol
712 formation. Resolving these links require more quantitative studies linking of the quality and quantity
713 of cyanobacterial blooms to the strength of emissions and to production of aerosol precursors. More
714 studies partitioning the influence of pelagic cyanobacterial blooms and influence of coastal
715 macroalgae on new particle formations would need to be undertaken.



716

717 *Data availability*

718 Mass spectrometer and air ion spectrometer data related to this article are available upon request to
719 the corresponding author. Rest of the data are available for download from
720 <https://avaa.tdata.fi/web/smart/smear>.

721 *Supplement*

722 The supplement related to this article is available online at:

723

724 *Author contributions*

725 RCT and TJ, MS designed the experiment, MS, LB, NS, YJT, TC, YJ, JL, ML were involved in the
726 instrument installations and performed calibrations, RCT, collected, processed, analyzed and
727 interpreted the mass spectrometric data. TC, JS, JL, RCT and ML collected and processed the particle
728 data. RCT, LD and KL interpreted the particle data. LD, LB, LQ and XCH performed the calculations.
729 MS, RCT, TJ and MK conceptualized the idea of connecting marine biology and atmospheric
730 processes. AN improvised the marine biology section of the paper. CX carried out Flexpart analysis.
731 MM contributed to the satellite data procurement and its interpretation. All authors contributed
732 commented on the manuscript and improvised the data interpretation.

733

734 *Acknowledgements*

735 We thank the ACTRIS CiGAS-UHEL calibration center for providing facility for CI-API-TOF
736 calibration and INAR technical staff for support during the entire experiment. We acknowledge
737 Finnish Meteorological Institute for providing open access to oceanographic data used in this study.
738 Financial support: This work was supported by the European Research Council (ERC) under the
739 European Union's Horizon 2020 research and innovation programme (GASPARCON, grant
740 agreement no. 714621) and by the Finnish Academy (grant agreement no. 334514). We also
741 acknowledge Jane and Aatos Erkko Foundation, ERC ATM-GTP, Flagship ACCC and Aerosols,
742 clouds and trace gases infrastructure (ACTRIS) for funding support.

743

744 *Competing Interests:* The authors declare that there are no conflict of interests

745

746 **References**

747 Allan, J. D., Williams, P. I., Najera, J., Whitehead, J. D., Flynn, M. J., Taylor, J. W., Liu, D., Darbyshire, E.,
748 Carpenter, L. J., Chance, R., Andrews, S. J., Hackenberg, S. C. and McFiggans, G.: Iodine observed in
749 new particle formation events in the Arctic atmosphere during ACCACIA, *Atmos. Chem. Phys.*, 15(10),



- 750 5599–5609, doi:10.5194/acp-15-5599-2015, 2015.
- 751 Almeida, J., Schobesberger, S., Kürten, A., Ortega, I. K., Kupiainen-Määttä, O., Praplan, A. P., Adamov, A.,
752 Amorim, A., Bianchi, F., Breitenlechner, M., David, A., Dommen, J., Donahue, N. M., Downard, A.,
753 Dunne, E., Duplissy, J., Ehrhart, S., Flagan, R. C., Franchin, A., Guida, R., Hakala, J., Hansel, A.,
754 Heinritzi, M., Henschel, H., Jokinen, T., Junninen, H., Kajos, M., Kangasluoma, J., Keskinen, H., Kupc,
755 A., Kurtén, T., Kvashin, A. N., Laaksonen, A., Lehtipalo, K., Leiminger, M., Leppä, J., Loukonen, V.,
756 Makhmutov, V., Mathot, S., McGrath, M. J., Nieminen, T., Olenius, T., Onnela, A., Petäjä, T.,
757 Riccobono, F., Riipinen, I., Rissanen, M., Rondo, L., Ruuskanen, T., Santos, F. D., Sarnela, N.,
758 Schallhart, S., Schnitzhofer, R., Seinfeld, J. H., Simon, M., Sipilä, M., Stozhkov, Y., Stratmann, F.,
759 Tomé, A., Tröstl, J., Tsagkogeorgas, G., Vaattovaara, P., Viisanen, Y., Virtanen, A., Vrtala, A., Wagner,
760 P. E., Weingartner, E., Wex, H., Williamson, C., Wimmer, D., Ye, P., Yli-Juuti, T., Carslaw, K. S.,
761 Kulmala, M., Curtius, J., Baltensperger, U., Worsnop, D. R., Vehkamäki, H. and Kirkby, J.: Molecular
762 understanding of sulphuric acid-amine particle nucleation in the atmosphere, *Nature*, 502(7471), 359–
763 363, doi:10.1038/nature12663, 2013.
- 764 Andersen, J. H., Carstensen, J., Conley, D. J., Dromph, K., Fleming-Lehtinen, V., Gustafsson, B. G., Josefson,
765 A. B., Norkko, A., Villnäs, A. and Murray, C.: Long-term temporal and spatial trends in eutrophication
766 status of the Baltic Sea, *Biol. Rev.*, doi:10.1111/brv.12221, 2017.
- 767 Ar Gall, E., Küpper, F. C. and Kloareg, B.: A survey of iodine content in *Laminaria digitata*, *Bot. Mar.*,
768 doi:10.1515/BOT.2004.004, 2004.
- 769 Artaxo, P., Rizzo, L. V., Brito, J. F., Barbosa, H. M. J., Arana, A., Sena, E. T., Cirino, G. G., Bastos, W.,
770 Martin, S. T. and Andreae, M. O.: Atmospheric aerosols in Amazonia and land use change: From natural
771 biogenic to biomass burning conditions, *Faraday Discuss.*, 165, 203–235, doi:10.1039/c3fd00052d,
772 2013.
- 773 Attard, K. M., Rodil, I. F., Berg, P., Norkko, J., Norkko, A. and Glud, R. N.: Seasonal metabolism and carbon
774 export potential of a key coastal habitat: The perennial canopy-forming macroalga *Fucus vesiculosus*,
775 *Limnol. Oceanogr.*, doi:10.1002/lno.11026, 2019.
- 776 Baalbaki, R., Pikridas, M., Jokinen, T., Laurila, T., Dada, L., Bezantakos, S., Ahonen, L., Neitola, K., Maisser,
777 A., Bimenyimana, E., Christodoulou, A., Unga, F., Savvides, C., Lehtipalo, K., Kangasluoma, J.,
778 Biskos, G., Petäjä, T., Kerminen, V. M., Sciare, J. and Kulmala, M.: Towards understanding the
779 characteristics of new particle formation in the Eastern Mediterranean, *Atmos. Chem. Phys.*,
780 doi:10.5194/acp-21-9223-2021, 2021.
- 781 Baccarini, A., Karlsson, L., Dommen, J., Duplessis, P., Vüllers, J., Brooks, I. M., Saiz-Lopez, A., Salter, M.,
782 Tjernström, M., Baltensperger, U., Zieger, P. and Schmale, J.: Frequent new particle formation over the
783 high Arctic pack ice by enhanced iodine emissions, *Nat. Commun.*, doi:10.1038/s41467-020-18551-0,
784 2020.
- 785 Beck, L. J., Sarnela, N., Junninen, H., Hoppe, C. J. M., Garmash, O., Bianchi, F., Riva, M., Rose, C., Peräkylä,
786 O., Wimmer, D., Kausiala, O., Jokinen, T., Ahonen, L., Mikkilä, J., Hakala, J., He, X. C., Kontkanen,



- 787 J., Wolf, K. K. E., Cappelletti, D., Mazzola, M., Traversi, R., Petroselli, C., Viola, A. P., Vitale, V.,
788 Lange, R., Massling, A., Nøjgaard, J. K., Krejci, R., Karlsson, L., Zieger, P., Jang, S., Lee, K., Vakkari,
789 V., Lampilahti, J., Thakur, R. C., Leino, K., Kangasluoma, J., Duplissy, E. M., Siivola, E., Marbouti,
790 M., Tham, Y. J., Saiz-Lopez, A., Petäjä, T., Ehn, M., Worsnop, D. R., Skov, H., Kulmala, M., Kerminen,
791 V. M. and Sipilä, M.: Differing Mechanisms of New Particle Formation at Two Arctic Sites, *Geophys.*
792 *Res. Lett.*, doi:10.1029/2020GL091334, 2021.
- 793 Benson, D. R., Young, L. H., Kameel, F. R. and Lee, S. H.: Laboratory-measured nucleation rates of sulfuric
794 acid and water binary homogeneous nucleation from the SO₂ + OH reaction, *Geophys. Res. Lett.*,
795 35(11), 1–6, doi:10.1029/2008GL033387, 2008.
- 796 Berresheim, H., Elste, T., Tremmel, H. G., Allen, A. G., Hansson, H. C., Rosman, K., Dal Maso, M., Mäkelä,
797 J. M., Kulmala, M. and O’Dowd, C. D.: Gas-aerosol relationships of H₂SO₄, MSA, and OH:
798 Observations in the coastal marine boundary layer at Mace Head, Ireland, *J. Geophys. Res. Atmos.*,
799 107(19), 1–12, doi:10.1029/2000JD000229, 2002.
- 800 Bianchi, F., Tröstl, J., Junninen, H., Frege, C., Henne, S., Hoyle, C. R., Molteni, U., Herrmann, E., Adamov,
801 A., Bukowiecki, N., Chen, X., Duplissy, J., Gysel, M., Hutterli, M., Kangasluoma, J., Kontkanen, J.,
802 Kürten, A., Manninen, H. E., Münch, S., Peräkylä, O., Petäjä, T., Rondo, L., Williamson, C.,
803 Weingartner, E., Curtius, J., Worsnop, D. R., Kulmala, M., Dommen, J. and Baltensperger, U.: New
804 particle formation in the free troposphere: A question of chemistry and timing, *Science* (80-.),
805 352(6289), 1109–1112, doi:10.1126/science.aad5456, 2016.
- 806 Bianchi, F., Junninen, H., Bigi, A., Sinclair, V. A., Dada, L., Hoyle, C. R., Zha, Q., Yao, L., Ahonen, L. R.,
807 Bonasoni, P., Buenrostro Mazon, S., Hutterli, M., Laj, P., Lehtipalo, K., Kangasluoma, J., Kerminen,
808 V. M., Kontkanen, J., Marinoni, A., Mirme, S., Molteni, U., Petäjä, T., Riva, M., Rose, C., Sellegri, K.,
809 Yan, C., Worsnop, D. R., Kulmala, M., Baltensperger, U. and Dommen, J.: Biogenic particles formed
810 in the Himalaya as an important source of free tropospheric aerosols, *Nat. Geosci.*, doi:10.1038/s41561-
811 020-00661-5, 2020.
- 812 Bigg, E. K. and Turvey, D. E.: Sources of atmospheric particles over Australia, *Atmos. Environ.*, 12(8), 1643–
813 1655, doi:10.1016/0004-6981(78)90313-X, 1978.
- 814 Boy, M., Karl, T., Turnipseed, A., Mauldin, R. L., Kosciuch, E., Greenberg, J., Rathbone, J., Smith, J., Held,
815 A., Barsanti, K., Wehner, B., Bauer, S., Wiedensohler, A., Bonn, B., Kulmala, M. and Guenther, A.:
816 New particle formation in the front range of the Colorado Rocky Mountains, *Atmos. Chem. Phys.*, 8(6),
817 1577–1590, doi:10.5194/acp-8-1577-2008, 2008.
- 818 Buenrostro Mazon, S., Kontkanen, J., Manninen, H. E., Nieminen, T., Kerminen, V. M. and Kulmala, M.: A
819 long-term comparison of nighttime cluster events and daytime ion formation in a boreal forest, *Boreal*
820 *Environ. Res.*, 21(3–4), 242–261, 2016.
- 821 Cai, R. and Jiang, J.: A new balance formula to estimate new particle formation rate: Reevaluating the effect
822 of coagulation scavenging, *Atmos. Chem. Phys.*, 17(20), 12659–12675, doi:10.5194/acp-17-12659-
823 2017, 2017.



- 824 Chan, T., Cai, R., Ahonen, L. R., Liu, Y., Zhou, Y., Vanhanen, J., Dada, L., Chao, Y., Liu, Y., Wang, L.,
825 Kulmala, M. and Kangasluoma, J.: Assessment of particle size magnifier inversion methods to obtain
826 the particle size distribution from atmospheric measurements, *Atmos. Meas. Tech.*, 13(9), 4885–4898,
827 doi:10.5194/amt-13-4885-2020, 2020.
- 828 Chen, D., Wang, W., Li, D. and Wang, W.: Atmospheric implication of synergy in methanesulfonic acid-base
829 trimers: A theoretical investigation, *RSC Adv.*, 10(9), 5173–5182, doi:10.1039/c9ra08760e, 2020.
- 830 Chen, H., Ezell, M. J., Arquero, K. D., Varner, M. E., Dawson, M. L., Gerber, R. B. and Finlayson-Pitts, B. J.:
831 New particle formation and growth from methanesulfonic acid, trimethylamine and water, *Phys. Chem.*
832 *Chem. Phys.*, 17(20), 13699–13709, doi:10.1039/c5cp00838g, 2015.
- 833 Chen, H., Varner, M. E., Gerber, R. B. and Finlayson-Pitts, B. J.: Reactions of Methanesulfonic Acid with
834 Amines and Ammonia as a Source of New Particles in Air, *J. Phys. Chem. B*, 120(8), 1526–1536,
835 doi:10.1021/acs.jpcc.5b07433, 2016.
- 836 Croft, B., Martin, R. V., Richard Leitch, W., Tunved, P., Breider, T. J., D’Andrea, S. D. and Pierce, J. R.:
837 Processes controlling the annual cycle of Arctic aerosol number and size distributions, *Atmos. Chem.*
838 *Phys.*, 16(6), 3665–3682, doi:10.5194/acp-16-3665-2016, 2016.
- 839 Dada, L., Paasonen, P., Nieminen, T., Buenrostro Mazon, S., Kontkanen, J., Peräkylä, O., Lehtipalo, K.,
840 Hussein, T., Petäjä, T., Kerminen, V. M., Bäck, J. and Kulmala, M.: Long-term analysis of clear-sky
841 new particle formation events and nonevents in Hyytiälä, *Atmos. Chem. Phys.*, doi:10.5194/acp-17-
842 6227-2017, 2017.
- 843 Dada, L., Chellapermal, R., Buenrostro Mazon, S., Paasonen, P., Lampilahti, J., E Manninen, H., Junninen,
844 H., Petäjä, T., Kerminen, V. M. and Kulmala, M.: Refined classification and characterization of
845 atmospheric new-particle formation events using air ions, *Atmos. Chem. Phys.*, 18(24), 17883–17893,
846 doi:10.5194/acp-18-17883-2018, 2018.
- 847 Dada, L., Lehtipalo, K., Kontkanen, J., Nieminen, T., Baalbaki, R., Ahonen, L., Duplissy, J., Yan, C., Chu, B.,
848 Petäjä, T., Lehtinen, K., Kerminen, V. M., Kulmala, M. and Kangasluoma, J.: Formation and growth of
849 sub-3-nm aerosol particles in experimental chambers, *Nat. Protoc.*, 15(3), 1013–1040,
850 doi:10.1038/s41596-019-0274-z, 2020a.
- 851 Dada, L., Ylivinkka, I., Baalbaki, R., Li, C., Guo, Y., Yan, C., Yao, L., Sarnela, N., Jokinen, T., Daellenbach,
852 K. R., Yin, R., Deng, C., Chu, B., Nieminen, T., Wang, Y., Lin, Z., Thakur, R. C., Kontkanen, J.,
853 Stolzenburg, D., Sipilä, M., Hussein, T., Paasonen, P., Bianchi, F., Salma, I., Weidinger, T., Pikridas,
854 M., Sciare, J., Jiang, J., Liu, Y., Petäjä, T., Kerminen, V. M. and Kulmala, M.: Sources and sinks driving
855 sulfuric acid concentrations in contrasting environments: Implications on proxy calculations, *Atmos.*
856 *Chem. Phys.*, doi:10.5194/acp-20-11747-2020, 2020b.
- 857 Dal Maso, M., Kulmala, M., Lehtinen, K. E. J., Mäkelä, J. M., Aalto, P. and O’Dowd, C. D.: Condensation and
858 coagulation sinks and formation of nucleation mode particles in coastal and boreal forest boundary
859 layers, *J. Geophys. Res. Atmos.*, 107(19), 1–22, doi:10.1029/2001JD001053, 2002.
- 860 Dal Maso, M., Kulmala, M., Riipinen, I., Wagner, R., Hussein, T., Aalto, P. P. and Lehtinen, K. E. J.:



- 861 Formation and growth of fresh atmospheric aerosols: Eight years of aerosol size distribution data from
862 SMEAR II, Hyytiälä, Finland, *Boreal Environ. Res.*, 10(5), 323–336, 2005.
- 863 Dal Maso, M., Liao, L., Wildt, J., Kiendler-Scharr, A., Kleist, E., Tillmann, R., Sipilä, M., Hakala, J.,
864 Lehtipalo, K., Ehn, M., Kerminen, V. M., Kulmala, M., Worsnop, D. and Mentel, T.: A chamber study
865 of the influence of boreal BVOC emissions and sulfuric acid on nanoparticle formation rates at ambient
866 concentrations, *Atmos. Chem. Phys.*, 16(4), 1955–1970, doi:10.5194/acp-16-1955-2016, 2016.
- 867 Deng, C., Fu, Y., Dada, L., Yan, C., Cai, R., Yang, D., Zhou, Y., Yin, R., Lu, Y., Li, X., Qiao, X., Fan, X.,
868 Nie, W., Kontkanen, J., Kangasluoma, J., Chu, B., Ding, A., Kerminen, V. M., Paasonen, P., Worsnop,
869 D. R., Bianchi, F., Liu, Y., Zheng, J., Wang, L., Kulmala, M. and Jiang, J.: Seasonal characteristics of
870 new particle formation and growth in urban Beijing, *Environ. Sci. Technol.*, 54(14), 8547–8557,
871 doi:10.1021/acs.est.0c00808, 2020.
- 872 Dowd, C. D. O., Lowe, J. A., Smith, M. H., Davison, B., Hewitt, C. N. and Harrison, R. M.: Biogenic sulphur
873 emissions and inferred non-sea-salt-sulphate particularly during Events of new particle formation were
874 Instrumentation and Cruise Summary, Atlantic, 102(DII), 1997.
- 875 Du, W., Dada, L., Zhao, J., Chen, X., Daellenbach, K. R., Xie, C., Wang, W., He, Y., Cai, J., Yao, L., Zhang,
876 Y., Wang, Q., Xu, W., Wang, Y., Tang, G., Cheng, X., Kokkonen, T. V., Zhou, W., Yan, C., Chu, B.,
877 Zha, Q., Hakala, S., Kurppa, M., Järvi, L., Liu, Y., Li, Z., Ge, M., Fu, P., Nie, W., Bianchi, F., Petäjä,
878 T., Paasonen, P., Wang, Z., Worsnop, D. R., Kerminen, V. M., Kulmala, M. and Sun, Y.: A 3D study
879 on the amplification of regional haze and particle growth by local emissions, *npj Clim. Atmos. Sci.*,
880 doi:10.1038/s41612-020-00156-5, 2021.
- 881 Duplissy, J., Merikanto, J., Franchin, A., Tsagkogeorgas, G., Kangasluoma, J., Wimmer, D., Vuollekoski, H.,
882 Schobesberger, S., Lehtipalo, K., Flagan, R. C., Brus, D., Donahue, N. M., Vehkamäki, H., Almeida, J.,
883 Amorim, A., Barmet, P., Bianchi, F., Breitenlechner, M., Dunne, E. M., Guida, R., Henschel, H.,
884 Junninen, H., Kirkby, J., Kürten, A., Kupc, A., Määttänen, A., Makhmutov, V., Mathot, S., Nieminen,
885 T., Onnela, A., Praplan, A. P., Riccobono, F., Rondo, L., Steiner, G., Tome, A., Walther, H.,
886 Baltensperger, U., Carslaw, K. S., Dommen, J., Hansel, A., Petäjä, T., Sipilä, M., Stratmann, F., Vrtala,
887 A., Wagner, P. E., Worsnop, D. R., Curtius, J. and Kulmala, M.: *Journal of Geophysical Research :
888 Atmospheres*, , 1752–1775, doi:10.1002/2015JD023538.Effect, 2016.
- 889 Eisele, Fred L; Tanner, D. : Measurement of the gas phase concentration of H₂SO₄ and Methane sulphonic
890 acid and estimates of H₂SO₄ production and Loss in Atmosphere, , 98(93), 9001–9010, 1993.
- 891 Eisele, F. L., Lovejoy, E. R., Kosciuch, E., Moore, K. F., Mauldin, I. L., Smith, J. N., McMurry, P. H. and
892 Iida, K.: Negative atmospheric ions and their potential role in ion-induced nucleation, *J. Geophys. Res.*
893 *Atmos.*, 111(4), doi:10.1029/2005JD006568, 2006.
- 894 Fiedler, V., Dal Maso, M., Boy, M., Aufmhoff, H., Hoffmann, J., Schuck, T., Birmili, W., Hanke, M., Uecker,
895 J., Arnold, F. and Kulmala, M.: The contribution of sulphuric acid to atmospheric particle formation and
896 growth: A comparison between boundary layers in Northern and Central Europe, *Atmos. Chem. Phys.*,
897 5(7), 1773–1785, doi:10.5194/acp-5-1773-2005, 2005.



- 898 Flanagan, R. J., Geever, M. and O'Dowd, C. D.: Direct measurements of new-particle fluxes in the coastal
899 environment, *Environ. Chem.*, 2(4), 256–259, doi:10.1071/EN05069, 2005.
- 900 Funkey, C. P., Conley, D. J., Reuss, N. S., Humborg, C., Jilbert, T. and Slomp, C. P.: Hypoxia sustains
901 cyanobacteria blooms in the Baltic Sea, *Environ. Sci. Technol.*, doi:10.1021/es404395a, 2014.
- 902 Glasoe, W. A., Volz, K., Panta, B., Freshour, N., Bachman, R., Hanson, D. R., McMurry, P. H. and Jen, C.:
903 Sulfuric acid nucleation: An experimental study of the effect of seven bases, *J. Geophys. Res.*,
904 doi:10.1002/2014JD022730, 2015.
- 905 He, X. C., Iyer, S., Sipilä, M., Ylisirniö, A., Peltola, M., Kontkanen, J., Baalbaki, R., Simon, M., Kürten, A.,
906 Tham, Y. J., Pesonen, J., Ahonen, L. R., Amanatidis, S., Amorim, A., Baccarini, A., Beck, L., Bianchi,
907 F., Brilke, S., Chen, D., Chiu, R., Curtius, J., Dada, L., Dias, A., Dommen, J., Donahue, N. M., Duplissy,
908 J., El Haddad, I., Finkenzeller, H., Fischer, L., Heinritzi, M., Hofbauer, V., Kangasluoma, J., Kim, C.,
909 Koenig, T. K., Kubečka, J., Kvashnin, A., Lamkaddam, H., Lee, C. P., Leiminger, M., Li, Z.,
910 Makhmutov, V., Xiao, M., Marten, R., Nie, W., Onnela, A., Partoll, E., Petäjä, T., Salo, V. T.,
911 Schuchmann, S., Steiner, G., Stolzenburg, D., Stozhkov, Y., Tauber, C., Tomé, A., Väisänen, O.,
912 Vazquez-Pufleau, M., Volkamer, R., Wagner, A. C., Wang, M., Wang, Y., Wimmer, D., Winkler, P.
913 M., Worsnop, D. R., Wu, Y., Yan, C., Ye, Q., Lehtinen, K., Nieminen, T., Manninen, H. E., Rissanen,
914 M., Schobesberger, S., Lehtipalo, K., Baltensperger, U., Hansel, A., Kerminen, V. M., Flagan, R. C.,
915 Kirkby, J., Kurtén, T. and Kulmala, M.: Determination of the collision rate coefficient between charged
916 iodine acid clusters and iodine acid using the appearance time method, *Aerosol Sci. Technol.*,
917 doi:10.1080/02786826.2020.1839013, 2021a.
- 918 He, X. C., Tham, Y. J., Dada, L., Wang, M., Finkenzeller, H., Stolzenburg, D., Iyer, S., Simon, M., Kürten,
919 A., Shen, J., Rörup, B., Rissanen, M., Schobesberger, S., Baalbaki, R., Wang, D. S., Koenig, T. K.,
920 Jokinen, T., Sarnela, N., Beck, L. J., Almeida, J., Amanatidis, S., Amorim, A., Ataei, F., Baccarini, A.,
921 Bertozzi, B., Bianchi, F., Brilke, S., Caudillo, L., Chen, D., Chiu, R., Chu, B., Dias, A., Ding, A.,
922 Dommen, J., Duplissy, J., Haddad, I. El, Carracedo, L. G., Granzin, M., Hansel, A., Heinritzi, M.,
923 Hofbauer, V., Junninen, H., Kangasluoma, J., Kempainen, D., Kim, C., Kong, W., Krechmer, J. E.,
924 Kvashin, A., Laitinen, T., Lamkaddam, H., Lee, C. P., Lehtipalo, K., Leiminger, M., Li, Z., Makhmutov,
925 V., Manninen, H. E., Marie, G., Marten, R., Mathot, S., Mauldin, R. L., Mentler, B., Möhler, O., Müller,
926 T., Nie, W., Onnela, A., Petäjä, T., Pfeifer, J., Philippov, M., Ranjithkumar, A., Saiz-Lopez, A., Salma,
927 I., Scholz, W., Schuchmann, S., Schulze, B., Steiner, G., Stozhkov, Y., Tauber, C., Tomé, A., Thakur,
928 R. C., Väisänen, O., Vazquez-Pufleau, M., Wagner, A. C., Wang, Y., Weber, S. K., Winkler, P. M., Wu,
929 Y., Xiao, M., Yan, C., Ye, Q., Ylisirniö, A., Zauner-Wieczorek, M., Zha, Q., Zhou, P., Flagan, R. C.,
930 Curtius, J., Baltensperger, U., Kulmala, M., Kerminen, V. M., Kurtén, T., et al.: Role of iodine oxoacids
931 in atmospheric aerosol nucleation, *Science* (80-.), doi:10.1126/science.abe0298, 2021b.
- 932 Hoffmann, E. H., Tilgner, A., Schrödner, R., Bräuer, P., Wolke, R. and Herrmann, H.: An advanced modeling
933 study on the impacts and atmospheric implications of multiphase dimethyl sulfide chemistry, *Proc. Natl.*
934 *Acad. Sci. U. S. A.*, doi:10.1073/pnas.1606320113, 2016.



- 935 Huang, R.-J., Seitz, K., Buxmann, J., Poehler, D., Hornsby, K. E., Carpenter, L. J., Platt, U. and Hoffmann,
936 T.: In situ measurements of molecular iodine in the marine boundary layer: the link to macroalgae and
937 the implications for O₃, IO, OIO and NO_x, Atmos.
938 Chem. Phys. Discuss., 10(1), 361–390, doi:10.5194/acpd-10-361-2010, 2010.
- 939 Huang, R. J., Thorenz, U. R., Kundel, M., Venables, D. S., Ceburnis, D., Ho, K. F., Chen, J., Vogel, A. L.,
940 Küpper, F. C., Smyth, P. P. A., Nitschke, U., Stengel, D. B., Berresheim, H., O’Dowd, C. D. and
941 Hoffmann, T.: The seaweeds *Fucus vesiculosus* and *Ascophyllum nodosum* are significant contributors
942 to coastal iodine emissions, Atmos. Chem. Phys., 13(10), 5255–5264, doi:10.5194/acp-13-5255-2013,
943 2013.
- 944 Iida, K., Stolzenburg, M. R., McMurry, P. H. and Smith, J. N.: Estimating nanoparticle growth rates from size-
945 dependent charged fractions: Analysis of new particle formation events in Mexico City, J. Geophys.
946 Res. Atmos., 113(5), 1–15, doi:10.1029/2007JD009260, 2008.
- 947 Jang, E., Park, K. T., Jun Yoon, Y., Kim, T. W., Hong, S. B., Becagli, S., Traversi, R., Kim, J. and Gim, Y.:
948 New particle formation events observed at the King Sejong Station, Antarctic Peninsula - Part 2: Link
949 with the oceanic biological activities, Atmos. Chem. Phys., 19(11), 7595–7608, doi:10.5194/acp-19-
950 7595-2019, 2019.
- 951 Jokinen, T., Sipilä, M., Junninen, H., Ehn, M., Lönn, G., Hakala, J., Petäjä, T., Mauldin, R. L., Kulmala, M.
952 and Worsnop, D. R.: Atmospheric sulphuric acid and neutral cluster measurements using CI-API-TOF,
953 Atmos. Chem. Phys., 12(9), 4117–4125, doi:10.5194/acp-12-4117-2012, 2012.
- 954 Jokinen, T., Sipilä, M., Kontkanen, J., Vakkari, V., Tisler, P., Duplissy, E. M., Junninen, H., Kangasluoma, J.,
955 Manninen, H. E., Petäjä, T., Kulmala, M., Worsnop, D. R., Kirkby, J., Virkkula, A. and Kerminen, V.
956 M.: Ion-induced sulfuric acid–ammonia nucleation drives particle formation in coastal Antarctica, Sci.
957 Adv., 4(11), 1–7, doi:10.1126/sciadv.aat9744, 2018.
- 958 Junninen, H., Ehn, M., Petäjä, T., Luosujärvi, L., Kotiaho, T., Kostianen, R., Rohner, U., Gonin, M., Fuhrer,
959 K., Kulmala, M. and Worsnop, D. R.: A high-resolution mass spectrometer to measure atmospheric ion
960 composition, Atmos. Meas. Tech. Discuss., 3(1), 599–636, doi:10.5194/amtd-3-599-2010, 2010.
- 961 Kahru, M. and Elmgren, R.: Multidecadal time series of satellite-detected accumulations of cyanobacteria in
962 the Baltic Sea, Biogeosciences, doi:10.5194/bg-11-3619-2014, 2014.
- 963 Kautsky, L. and Kautsky, N.: The Baltic Sea, including Bothnian Sea and Bothnian Bay, Seas Millenn. - an
964 Environ. Eval. - Vol. 1, 2000.
- 965 Keller, M. D., Bellows, W. K. and Guillard, R. R. L.: Dimethyl Sulfide Production in Marine Phytoplankton.,
966 1989.
- 967 Kettle, A. J. and Andreae, M. O.: Flux of dimethylsulfide from the oceans: A comparison of updated data sets
968 and flux models, J. Geophys. Res. Atmos., doi:10.1029/2000JD900252, 2000.
- 969 Kirkby, J., Curtius, J., Almeida, J., Dunne, E., Duplissy, J., Ehrhart, S., Franchin, A., Gagné, S., Ickes, L.,
970 Kürten, A., Kupc, A., Metzger, A., Riccobono, F., Rondo, L., Schobesberger, S., Tsagkogeorgas, G.,
971 Wimmer, D., Amorim, A., Bianchi, F., Breitenlechner, M., David, A., Dommen, J., Downard, A., Ehn,



- 972 M., Flagan, R. C., Haider, S., Hansel, A., Hauser, D., Jud, W., Junninen, H., Kreissl, F., Kvashin, A.,
973 Laaksonen, A., Lehtipalo, K., Lima, J., Lovejoy, E. R., Makhmutov, V., Mathot, S., Mikkilä, J.,
974 Minginette, P., Mogo, S., Nieminen, T., Onnela, A., Pereira, P., Petäjä, T., Schnitzhofer, R., Seinfeld, J.
975 H., Sipilä, M., Stozhkov, Y., Stratmann, F., Tomé, A., Vanhanen, J., Viisanen, Y., Vrtala, A., Wagner,
976 P. E., Walther, H., Weingartner, E., Wex, H., Winkler, P. M., Carslaw, K. S., Worsnop, D. R.,
977 Baltensperger, U. and Kulmala, M.: Role of sulphuric acid, ammonia and galactic cosmic rays in
978 atmospheric aerosol nucleation, *Nature*, 476(7361), 429–435, doi:10.1038/nature10343, 2011.
- 979 Kirkby, J., Duplissy, J., Sengupta, K., Frege, C., Gordon, H., Williamson, C., Heinritzi, M., Simon, M., Yan,
980 C., Almeida, J., Trostl, J., Nieminen, T., Ortega, I. K., Wagner, R., Adamov, A., Amorim, A.,
981 Bernhammer, A. K., Bianchi, F., Breitenlechner, M., Brilke, S., Chen, X., Craven, J., Dias, A., Ehrhart,
982 S., Flagan, R. C., Franchin, A., Fuchs, C., Guida, R., Hakala, J., Hoyle, C. R., Jokinen, T., Junninen, H.,
983 Kangasluoma, J., Kim, J., Krapf, M., Kurten, A., Laaksonen, A., Lehtipalo, K., Makhmutov, V., Mathot,
984 S., Molteni, U., Onnela, A., Perakyla, O., Piel, F., Petaja, T., Praplan, A. P., Pringle, K., Rap, A.,
985 Richards, N. A. D., Riipinen, I., Rissanen, M. P., Rondo, L., Sarnela, N., Schobesberger, S., Scott, C.
986 E., Seinfeld, J. H., Sipilä, M., Steiner, G., Stozhkov, Y., Stratmann, F., Tomé, A., Virtanen, A., Vogel,
987 A. L., Wagner, A. C., Wagner, P. E., Weingartner, E., Wimmer, D., Winkler, P. M., Ye, P., Zhang, X.,
988 Hansel, A., Dommen, J., Donahue, N. M., Worsnop, D. R., Baltensperger, U., Kulmala, M., Carslaw,
989 K. S. and Curtius, J.: Ion-induced nucleation of pure biogenic particles, *Nature*, 533(7604), 521–526,
990 doi:10.1038/nature17953, 2016.
- 991 Knutson, E. O. and Whitby, K. T.: Aerosol classification by electric mobility: apparatus, theory, and
992 applications, *J. Aerosol Sci.*, 6(6), 443–451, doi:10.1016/0021-8502(75)90060-9, 1975.
- 993 Knutson, E. O., Whitby, K. T., Fiedler, V., Dal Maso, M., Boy, M., Aufmhoff, H., Hoffmann, J., Schuck, T.,
994 Birmili, W., Hanke, M., Uecker, J., Arnold, F., Kulmala, M., Petäjä, T., Nieminen, T., Sipilä, M.,
995 Manninen, H. E., Lehtipalo, K., Dal Maso, M., Aalto, P. P., Junninen, H., Paasonen, P., Riipinen, I.,
996 Lehtinen, K. E. J., Laaksonen, A., Kerminen, V. M., Croft, B., Martin, R. V., Richard Leitch, W.,
997 Tunved, P., Breider, T. J., D’Andrea, S. D., Pierce, J. R., Glasoe, W. A., Volz, K., Panta, B., Freshour,
998 N., Bachman, R., Hanson, D. R., McMurry, P. H., Jen, C., Suikkanen, S., Pulina, S., Engström-Öst, J.,
999 Lehtiniemi, M., Lehtinen, S., Brutemark, A., Berresheim, H., Elste, T., Tremmel, H. G., Allen, A. G.,
1000 Hansson, H. C., Rosman, K., Dal Maso, M., Mäkelä, J. M., Kulmala, M., O’Dowd, C. D., Lehtinen, K.
1001 E. J., Kulmala, M., Manninen, H. E., Nieminen, T., Asmi, E., Gagné, S., Häkkinen, S., Lehtipalo, K.,
1002 Aalto, P. P., Vana, M., Mirme, A., Mirme, S., Hörrak, U., Plass-Dülmer, C., Stange, G., Kiss, G., Hoffer,
1003 A., Töro, N., Moerman, M., Henzing, B., De Leeuw, G., Brinkenberg, M., Kouvarakis, G. N.,
1004 Bougiatioti, A., Mihalopoulos, N., O’Dowd, C. D., Ceburnis, D., Arneth, A., Svenningsson, B.,
1005 Swietlicki, E., Tarozzi, L., Decesari, S., Facchini, M. C., Birmili, W., Sonntag, A., Wiedensohler, A.,
1006 Boulon, J., Sellegri, K., Laj, P., Gysel, M., Bukowiecki, N., Weingartner, E., et al.: Quantification of the
1007 volatility of secondary organic compounds in ultrafine particles during nucleation events, *Atmos. Chem.*
1008 *Phys.*, 10(4), 1–10, doi:10.1039/c9ra08760e, 2016.



- 1009 Kownacka, J., Calkiewicz, J. and Kornijów, R.: A turning point in the development of phytoplankton in the
1010 Vistula Lagoon (southern Baltic Sea) at the beginning of the 21st century, *Oceanologia*,
1011 doi:10.1016/j.oceano.2020.08.004, 2020.
- 1012 Kulmala, M., Toivonen, A., Mäkelä, J. M. and Laaksonen, A.: Analysis of the growth of nucleation mode
1013 particles observed in Boreal forest, *Tellus, Ser. B Chem. Phys. Meteorol.*,
1014 doi:10.3402/tellusb.v50i5.16229, 1998.
- 1015 Kulmala, M., Laakso, L., Lehtinen, K. E. J., Riipinen, I., Dal Maso, M., Anttila, T., Kerminen, V.-M., Hörrak,
1016 U., Vana, M. and Tammet, H.: Initial steps of aerosol growth, *Atmos. Chem. Phys.*, doi:10.5194/acp-4-
1017 2553-2004, 2004.
- 1018 Kulmala, M., Petäjä, T., Mönkkönen, P., Koponen, I. K., Dal Maso, M., Aalto, P. P., Lehtinen, K. E. J. and
1019 Kerminen, V. M.: On the growth nucleation mode particles: Source rates of condensable vapor in
1020 polluted and clean environments, *Atmos. Chem. Phys.*, 5(2), 409–416, doi:10.5194/acp-5-409-2005,
1021 2005.
- 1022 Kulmala, M., Petäjä, T., Nieminen, T., Sipilä, M., Manninen, H. E., Lehtipalo, K., Dal Maso, M., Aalto, P. P.,
1023 Junninen, H., Paasonen, P., Riipinen, I., Lehtinen, K. E. J., Laaksonen, A. and Kerminen, V. M.:
1024 Measurement of the nucleation of atmospheric aerosol particles, *Nat. Protoc.*, 7(9), 1651–1667,
1025 doi:10.1038/nprot.2012.091, 2012.
- 1026 Kulmala, M., Kontkanen, J., Junninen, H., Lehtipalo, K., Manninen, H. E., Nieminen, T., Petäjä, T., Sipilä,
1027 M., Schobesberger, S., Rantala, P., Franchin, A., Jokinen, T., Järvinen, E., Äijälä, M., Kangasluoma, J.,
1028 Hakala, J., Aalto, P. P., Paasonen, P., Mikkilä, J., Vanhanen, J., Aalto, J., Hakola, H., Makkonen, U.,
1029 Ruuskanen, T., Mauldin, R. L., Duplissy, J., Vehkamäki, H., Bäck, J., Kortelainen, A., Riipinen, I.,
1030 Kurtén, T., Johnston, M. V., Smith, J. N., Ehn, M., Mentel, T. F., Lehtinen, K. E. J., Laaksonen, A.,
1031 Kerminen, V. M. and Worsnop, D. R.: Direct observations of atmospheric aerosol nucleation, *Science*
1032 (80), 339(6122), 943–946, doi:10.1126/science.1227385, 2013.
- 1033 Kulmala, M., Petäjä, T., Kerminen, V. M., Kujansuu, J., Ruuskanen, T., Ding, A., Nie, W., Hu, M., Wang, Z.,
1034 Wu, Z., Wang, L. and Worsnop, D. R.: On secondary new particle formation in China, *Front. Environ.*
1035 *Sci. Eng.*, 10(5), 1–10, doi:10.1007/s11783-016-0850-1, 2016.
- 1036 Kulmala, M., Kerminen, V. M., Petäjä, T., Ding, A. J. and Wang, L.: Atmospheric gas-to-particle conversion:
1037 Why NPF events are observed in megacities?, *Faraday Discuss.*, 200, 271–288,
1038 doi:10.1039/c6fd00257a, 2017.
- 1039 Kuosa, H., Fleming-Lehtinen, V., Lehtinen, S., Lehtiniemi, M., Nygård, H., Raateoja, M., Raitaniemi, J.,
1040 Tuimala, J., Uusitalo, L. and Suikkanen, S.: A retrospective view of the development of the Gulf of
1041 Bothnia ecosystem, *J. Mar. Syst.*, 167, 78–92, doi:10.1016/j.jmarsys.2016.11.020, 2017.
- 1042 Küpper, F. C., Schweigert, N., Ar Gall, E., Legendre, J. M., Vilter, H. and Kloareg, B.: Iodine uptake in
1043 Laminariales involves extracellular, haloperoxidase-mediated oxidation of iodide, *Planta*,
1044 doi:10.1007/s004250050469, 1998.
- 1045 Kürten, A., Jokinen, T., Simon, M., Sipilä, M., Sarnela, N., Junninen, H., Adamov, A., Almeida, J., Amorim,



- 1046 A., Bianchi, F., Breitenlechner, M., Dommen, J., Donahue, N. M., Duplissy, J., Ehrhart, S., Flagan, R.
1047 C., Franchin, A., Hakala, J., Hansel, A., Heinritzi, M., Hutterli, M., Kangasluoma, J., Kirkby, J.,
1048 Laaksonen, A., Lehtipalo, K., Leiminger, M., Makhmutov, V., Mathot, S., Onnela, A., Petäjä, T.,
1049 Praplan, A. P., Riccobono, F., Rissanen, M. P., Rondo, L., Schobesberger, S., Seinfeld, J. H., Steiner,
1050 G., Tomé, A., Tröstl, J., Winkler, P. M., Williamson, C., Wimmer, D., Ye, P., Baltensperger, U.,
1051 Carslaw, K. S., Kulmala, M., Worsnop, D. R. and Curtius, J.: Neutral molecular cluster formation of
1052 sulfuric acid-dimethylamine observed in real time under atmospheric conditions, *Proc. Natl. Acad. Sci.*
1053 *U. S. A.*, 111(42), 15019–15024, doi:10.1073/pnas.1404853111, 2014.
- 1054 Kürten, A., Münch, S., Rondo, L., Bianchi, F., Duplissy, J., Jokinen, T., Junninen, H., Sarnela, N.,
1055 Schobesberger, S., Simon, M., Sipilä, M., Almeida, J., Amorim, A., Dommen, J., Donahue, N. M.,
1056 Dunne, E. M., Flagan, R. C., Franchin, A., Kirkby, J., Kupc, A., Makhmutov, V., Petäjä, T., Praplan, A.
1057 P., Riccobono, F., Steiner, G., Tomé, A., Tsagkogeorgas, G., Wagner, P. E., Wimmer, D., Baltensperger,
1058 U., Kulmala, M., Worsnop, D. R. and Curtius, J.: Thermodynamics of the formation of sulfuric acid
1059 dimers in the binary (H₂SO₄-H₂O) and ternary (H₂SO₄-H₂O-NH₃) system, *Atmos. Chem. Phys.*,
1060 15(18), 10701–10721, doi:10.5194/acp-15-10701-2015, 2015.
- 1061 Kürten, A., Bianchi, F., Almeida, J., Kupiainen-Määttä, O., Dunne, E. M., Duplissy, J., Williamson, C.,
1062 Barmet, P., Breitenlechner, M., Dommen, J., Donahue, N. M., Flagan, R. C., Franchin, A., Gordon, H.,
1063 Hakala, J., Hansel, A., Heinritzi, M., Ickes, L., Jokinen, T., Kangasluoma, J., Kim, J., Kirkby, J., Kupc,
1064 A., Lehtipalo, K., Leiminger, M., Makhmutov, V., Onnela, A., Ortega, I. K., Petäjä, T., Praplan, A. P.,
1065 Riccobono, F., Rissanen, M. P., Rondo, L., Schnitzhofer, R., Schobesberger, S., Smith, J. N., Steiner,
1066 G., Stozhkov, Y., Tomé, A., Tröstl, J., Tsagkogeorgas, G., Wagner, P. E., Wimmer, D., Ye, P.,
1067 Baltensperger, U., Carslaw, K., Kulmala, M. and Curtius, J.: Experimental particle formation rates
1068 spanning tropospheric sulfuric acid and ammonia abundances, ion production rates, and temperatures,
1069 *J. Geophys. Res.*, doi:10.1002/2015JD023908, 2016.
- 1070 Kyrö, E. M., Väänänen, R., Kerminen, V. M., Virkkula, A., Petäjä, T., Asmi, A., Dal Maso, M., Nieminen, T.,
1071 Juhola, S., Shcherbinin, A., Riipinen, I., Lehtipalo, K., Keronen, P., Aalto, P. P., Hari, P. and Kulmala,
1072 M.: Trends in new particle formation in eastern Lapland, Finland: Effect of decreasing sulfur emissions
1073 from Kola Peninsula, *Atmos. Chem. Phys.*, 14(9), 4383–4396, doi:10.5194/acp-14-4383-2014, 2014.
- 1074 Lehtipalo, K., Kontkanen, J., Kangasluoma, J., Franchin, A., Wimmer, D., Schobesberger, S., Junninen, H.,
1075 Petäjä, T., Sipilä, M., Worsnop, D. R., Kulmala, M., Lehtipalo, K., Mikkilä, J., Vanhanen, J., Leppä, J.
1076 and Worsnop, D. R.: Methods for determining particle size distribution and growth rates between 1 and
1077 3 nm using the Particle Size Magnifier, *Boreal Environ. Res.*, 19(September), 215–236, 2014.
- 1078 Leino, K., Nieminen, T., Manninen, H. E., Petäjä, T., Kerminen, V. M. and Kulmala, M.: Intermediate ions as
1079 a strong indicator of new particle formation bursts in boreal forest, *Boreal Environ. Res.*, 21(3–4), 274–
1080 286, 2016.
- 1081 Mahajan, A. S., Oetjen, H., Saiz-Lopez, A., Lee, J. D., McFiggans, G. B. and Plane, J. M. C.: Reactive iodine
1082 species in a semi-polluted environment, *Geophys. Res. Lett.*, 36(16), 6–11,



- 1083 doi:10.1029/2009GL038018, 2009.
- 1084 Mahajan, A. S., Sorribas, M., Martín, J. C. G., MacDonald, S. M., Gil, M., Plane, J. M. C. and Saiz-Lopez, A.:
1085 Concurrent observations of atomic iodine, molecular iodine and ultrafine particles in a coastal
1086 environment, *Atmos. Chem. Phys.*, 11(6), 2545–2555, doi:10.5194/acp-11-2545-2011, 2011.
- 1087 Manninen, H. E., Nieminen, T., Asmi, E., Gagné, S., Häkkinen, S., Lehtipalo, K., Aalto, P., Vana, M., Mirme,
1088 A., Mirme, S., Hörrak, U., Plass-Dülmer, C., Stange, G., Kiss, G., Hoffer, A., Töro, N., Moerman, M.,
1089 Henzing, B., De Leeuw, G., Brinkenberg, M., Kouvarakis, G. N., Bougiatioti, A., Mihalopoulos, N.,
1090 O’Dowd, C., Ceburnis, D., Arneth, A., Svenningsson, B., Swietlicki, E., Tarozzi, L., Decesari, S.,
1091 Facchini, M. C., Birmili, W., Sonntag, A., Wiedensohler, A., Boulon, J., Sellegri, K., Laj, P., Gysel, M.,
1092 Bukowiecki, N., Weingartner, E., Wehrle, G., Laaksonen, A., Hamed, A., Joutsensaari, J., Petäjä, T.,
1093 Kerminen, V. M. and Kulmala, M.: EUCAARI ion spectrometer measurements at 12 European sites-
1094 analysis of new particle formation events, *Atmos. Chem. Phys.*, 10(16), 7907–7927, doi:10.5194/acp-
1095 10-7907-2010, 2010.
- 1096 Mauldin, R. L., Eisele, F. L., Kosciuch, E., Shetter, R., Lefer, B., Buhr, M., Chen, G., Wang, P. and Davis, D.:
1097 *Oil J andjO (‘ D)*, , 28(19), 3629–3632, 2001.
- 1098 McFiggans, G., Coe, H., Burgess, R., Allan, J., Cubison, M., Alfarra, M. R., Saunders, R., Saiz-Lopez, A.,
1099 Plane, J. M. C., Wevill, D. J., Carpenter, L. J., Rickard, A. R. and Monks, P. S.: Direct evidence for
1100 coastal iodine particles from *Laminaria* macroalgae - Linkage to emissions of molecular iodine, *Atmos.*
1101 *Chem. Phys.*, 4(3), 701–713, doi:10.5194/acp-4-701-2004, 2004.
- 1102 McFiggans, G., Bale, C. S. E., Ball, S. M., Beames, J. M., Bloss, W. J., Carpenter, L. J., Dorsey, J., Dunk, R.,
1103 Flynn, M. J., Furneaux, K. L., Gallagher, M. W., Heard, D. E., Hollingsworth, A. M., Hornsby, K.,
1104 Ingham, T., Jones, C. E., Jones, R. L., Kramer, L. J., Langridge, J. M., Leblanc, C., LeCrane, J. P., Lee,
1105 J. D., Leigh, R. J., Longley, I., Mahajan, A. S., Monks, P. S., Oetjen, H., Orr-Ewing, A. J., Plane, J. M.
1106 C., Potin, P., Shillings, A. J. L., Thomas, F., Von Glasow, R., Wada, R., Whalley, L. K. and Whitehead,
1107 J. D.: Iodine-mediated coastal particle formation: An overview of the Reactive Halogens in the Marine
1108 boundary layer (RHAMBLE) Roscoff coastal study, *Atmos. Chem. Phys.*, 10(6), 2975–2999,
1109 doi:10.5194/acp-10-2975-2010, 2010.
- 1110 Meixner, F. X. and Yang, W. X.: Biogenic emissions of nitric oxide and nitrous oxide from arid and semi-arid
1111 land, in *Dryland Ecohydrology.*, 2006.
- 1112 Mirme, S. and Mirme, A.: The mathematical principles and design of the NAIS - A spectrometer for the
1113 measurement of cluster ion and nanometer aerosol size distributions, *Atmos. Meas. Tech.*, 6(4), 1061–
1114 1071, doi:10.5194/amt-6-1061-2013, 2013.
- 1115 Nieminen, T., Manninen, H. E., Sihto, S. L., Yli-Juuti, T., Mauldin, R. L., Petäjä, T., Riipinen, I., Kerminen,
1116 V. M. and Kulmala, M.: Connection of sulfuric acid to atmospheric nucleation in boreal forest, *Environ.*
1117 *Sci. Technol.*, 43(13), 4715–4721, doi:10.1021/es803152j, 2009.
- 1118 Nieminen, T., Lehtinen, K. E. J. and Kulmala, M.: Sub-10 nm particle growth by vapor condensation-effects
1119 of vapor molecule size and particle thermal speed, *Atmos. Chem. Phys.*, doi:10.5194/acp-10-9773-2010,



- 1120 2010.
- 1121 Nieminen, T., Asmi, A., Aalto, P. P., Keronen, P., Petäjä, T., Kulmala, M., Kerminen, V. M., Nieminen, T.
1122 and Dal Maso, M.: Trends in atmospheric new-particle formation: 16 years of observations in a boreal-
1123 forest environment, *Boreal Environ. Res.*, 19(September), 191–214, 2014.
- 1124 O’ Dowd, C. D., Jimenez, J. L., Bahreini, R., Flagan, R. C., Seinfeld, J. H., Hämerl, K., Pirjola, L., Kulmala,
1125 M. and Hoffmann, T.: Marine aerosol formation from biogenic iodine emissions, *Nature*, 417(6889),
1126 632–636, doi:10.1038/nature00775, 2002.
- 1127 Okuljar, M., Kuuluvainen, H., Kontkanen, J., Garmash, O., Olin, M., Niemi, J. V., Timonen, H., Kangasluoma,
1128 J., Tham, Y. J., Baalbaki, R., Sipilä, M., Salo, L., Lintusaari, H., Portin, H., Teinilä, K., Aurela, M., Dal
1129 Maso, M., Rönkkö, T., Petäjä, T. and Paasonen, P.: Measurement report: The influence of traffic and
1130 new particle formation on the size distribution of 1-800nm particles in Helsinki-a street canyon and an
1131 urban background station comparison, *Atmos. Chem. Phys.*, doi:10.5194/acp-21-9931-2021, 2021.
- 1132 Olin, M., Kuuluvainen, H., Aurela, M., Kalliokoski, J., Kuitinen, N., Isotalo, M., Timonen, H. J., Niemi, J.
1133 V., Rönkkö, T. and Dal Maso, M.: Traffic-originated nanocluster emission exceeds H₂SO₄-driven
1134 photochemical new particle formation in an urban area, *Atmos. Chem. Phys.*, 20(1), 1–13,
1135 doi:10.5194/acp-20-1-2020, 2020.
- 1136 Paasonen, P., Nieminen, T., Asmi, E., Manninen, H. E., Petäjä, T., Plass-Dülmer, C., Flentje, H., Birmili, W.,
1137 Wiedensohler, A., Hörrak, U., Metzger, A., Hamed, A., Laaksonen, A., Facchini, M. C., Kerminen, V.
1138 M. and Kulmala, M.: On the roles of sulphuric acid and low-volatility organic vapours in the initial steps
1139 of atmospheric new particle formation, *Atmos. Chem. Phys.*, 10(22), 11223–11242, doi:10.5194/acp-
1140 10-11223-2010, 2010.
- 1141 Peters, C., Pechtl, S., Stutz, J., Hebestreit, K., Hönninger, G., Heumann, K. G., Schwarz, A., Winterlik, J. and
1142 Platt, U.: Reactive and organic halogen species in three different European coastal environments, *Atmos.*
1143 *Chem. Phys.*, 5(12), 3357–3375, doi:10.5194/acp-5-3357-2005, 2005.
- 1144 Pierce, J. R., Riipinen, I., Kulmala, M., Ehn, M., Petäjä, T., Junninen, H., Worsnop, D. R. and Donahue, N.
1145 M.: Quantification of the volatility of secondary organic compounds in ultrafine particles during
1146 nucleation events, *Atmos. Chem. Phys.*, 11(17), 9019–9036, doi:10.5194/acp-11-9019-2011, 2011.
- 1147 Pisso, I., Sollum, E., Grythe, H., Kristiansen, N. I., Cassiani, M., Eckhardt, S., Arnold, D., Morton, D.,
1148 Thompson, R. L., Groot Zwaaftink, C. D., Evangeliou, N., Sodemann, H., Haimberger, L., Henne, S.,
1149 Brunner, D., Burkhardt, J. F., Fouilloux, A., Brioude, J., Philipp, A., Seibert, P. and Stohl, A.: The
1150 Lagrangian particle dispersion model FLEXPART version 10.4, *Geosci. Model Dev.*, doi:10.5194/gmd-
1151 12-4955-2019, 2019.
- 1152 Raso, A. R. W., Custard, K. D., May, N. W., Tanner, D., Newburn, M. K., Walker, L., Moore, R. J., Huey, L.
1153 G., Alexander, L., Shepson, P. B. and Pratt, K. A.: Active molecular iodine photochemistry in the Arctic,
1154 *Proc. Natl. Acad. Sci. U. S. A.*, 114(38), 10053–10058, doi:10.1073/pnas.1702803114, 2017.
- 1155 Riipinen, I., Yli-Juuti, T., Pierce, J. R., Petäjä, T., Worsnop, D. R., Kulmala, M. and Donahue, N. M.: The
1156 contribution of organics to atmospheric nanoparticle growth, *Nat. Geosci.*, 5(7), 453–458,



- 1157 doi:10.1038/ngeo1499, 2012.
- 1158 Riipinen, I., Yli-Juuti, T., Pierce, J. R., Petäjä, T., Worsnop, D. R., Kulmala, M. and Donahue, N. M.: The
1159 contribution of organics to atmospheric nanoparticle growth, *Nat. Geosci.*, doi:10.1038/ngeo1499,
1160 2012b.
- 1161 Rolph, G., Stein, A. and Stunder, B.: Real-time Environmental Applications and Display sYstem: READY,
1162 *Environ. Model. Softw.*, 95, 210–228, doi:10.1016/j.envsoft.2017.06.025, 2017.
- 1163 Rong, H., Liu, J., Zhang, Y., Du, L., Zhang, X. and Li, Z.: Nucleation mechanisms of iodic acid in clean and
1164 polluted coastal regions, *Chemosphere*, 253, 126743, doi:10.1016/j.chemosphere.2020.126743, 2020.
- 1165 Rose, C., Zha, Q., Dada, L., Yan, C., Lehtipalo, K., Junninen, H., Mazon, S. B., Jokinen, T., Sarnela, N., Sipilä,
1166 M., Petäjä, T., Kerminen, V. M., Bianchi, F. and Kulmala, M.: Observations of biogenic ion-induced
1167 cluster formation in the atmosphere, *Sci. Adv.*, 4(4), 1–11, doi:10.1126/sciadv.aar5218, 2018.
- 1168 Saiz-Lopez, A. and Plane, J. M. C.: Novel iodine chemistry in the marine boundary layer, *Geophys. Res. Lett.*,
1169 31(4), 1999–2002, doi:10.1029/2003GL019215, 2004.
- 1170 Saiz-Lopez, A., Plane, J. M. C., Baker, A. R., Carpenter, L. J., Von Glasow, R., Gómez Martín, J. C.,
1171 McFiggans, G. and Saunders, R. W.: Atmospheric chemistry of iodine, *Chem. Rev.*, 112(3), 1773–1804,
1172 doi:10.1021/cr200029u, 2012.
- 1173 Schagerström, E., Forslund, H., Kautsky, L., Pärnoja, M. and Kotta, J.: Does thalli complexity and biomass
1174 affect the associated flora and fauna of two co-occurring *Fucus* species in the Baltic Sea?, *Estuar. Coast.
1175 Shelf Sci.*, doi:10.1016/j.ecss.2014.08.022, 2014.
- 1176 Sipilä, M., Berndt, T., Petaja, T., Brus, D., Vanhanen, J., Stratmann, F., Patokoski, J., Mauldin, R. L.,
1177 Hyvärinen, A. P., Lihavainen, H. and Kulmala, M.: The role of sulfuric acid in atmospheric nucleation,
1178 *Science (80-.)*, 327(5970), 1243–1246, doi:10.1126/science.1180315, 2010.
- 1179 Sipilä, M.: Insights Into Atmospheric Nucleation. [online] Available from:
1180 <https://helda.helsinki.fi/bitstream/handle/10138/154171/insights.pdf?sequence=1>, 2010.
- 1181 Sipilä, M., Sarnela, N., Jokinen, T., Henschel, H., Junninen, H., Kontkanen, J., Richters, S., Kangasluoma, J.,
1182 Franchin, A., Peräkylä, O., Rissanen, M. P., Ehn, M., Vehkamäki, H., Kurten, T., Berndt, T., Petäjä, T.,
1183 Worsnop, D., Ceburnis, D., Kerminen, V. M., Kulmala, M. and O’Dowd, C.: Molecular-scale evidence
1184 of aerosol particle formation via sequential addition of HIO₃, *Nature*, 537(7621), 532–534,
1185 doi:10.1038/nature19314, 2016.
- 1186 Stein, A. F., Draxler, R. R., Rolph, G. D., Stunder, B. J. B., Cohen, M. D. and Ngan, F.: Noaa’s hysplit
1187 atmospheric transport and dispersion modeling system, *Bull. Am. Meteorol. Soc.*, 96(12), 2059–2077,
1188 doi:10.1175/BAMS-D-14-00110.1, 2015.
- 1189 Steinke, M., Hodapp, B., Subhan, R., Bell, T. G. and Martin-Creuzburg, D.: Flux of the biogenic volatiles
1190 isoprene and dimethyl sulfide from an oligotrophic lake, *Sci. Rep.*, doi:10.1038/s41598-017-18923-5,
1191 2018.
- 1192 Stohl, A., Forster, C., Frank, A., Seibert, P. and Wotawa, G.: Technical note: The Lagrangian particle
1193 dispersion model FLEXPART version 6.2, *Atmos. Chem. Phys.*, doi:10.5194/acp-5-2461-2005, 2005.



- 1194 Stolzenburg, D., Stolzenburg, D., Simon, M., Ranjithkumar, A., Kürten, A., Lehtipalo, K., Lehtipalo, K.,
1195 Gordon, H., Ehrhart, S., Finkenzeller, H., Pichelstorfer, L., Nieminen, T., He, X. C., Brilke, S., Xiao,
1196 M., Amorim, A., Baalbaki, R., Baccarini, A., Beck, L., Bräkling, S., Murillo, L. C., Chen, D., Chu, B.,
1197 Dada, L., Dias, A., Dommen, J., Duplissy, J., El Haddad, I., Fischer, L., Carracedo, L. G., Heinritzi, M.,
1198 Kim, C., Kim, C., Koenig, T. K., Kong, W., Lamkaddam, H., Lee, C. P., Leiminger, M., Leiminger, M.,
1199 Li, Z., Makhmutov, V., Manninen, H. E., Marie, G., Marten, R., Müller, T., Nie, W., Partoll, E., Petäjä,
1200 T., Pfeifer, J., Philippov, M., Rissanen, M. P., Rissanen, M. P., Rörup, B., Schobesberger, S.,
1201 Schuchmann, S., Shen, J., Sipilä, M., Steiner, G., Stozhkov, Y., Tauber, C., Tham, Y. J., Tomé, A.,
1202 Vazquez-Pufleau, M., Wagner, A. C., Wagner, A. C., Wang, M., Wang, Y., Weber, S. K., Wimmer, D.,
1203 Wimmer, D., Wlasits, P. J., Wu, Y., Ye, Q., Zauner-Wieczorek, M., Baltensperger, U., Carslaw, K. S.,
1204 Curtius, J., Donahue, N. M., Flagan, R. C., Hansel, A., Hansel, A., Kulmala, M., Lelieveld, J., Volkamer,
1205 R., Kirkby, J., Kirkby, J. and Winkler, P. M.: Enhanced growth rate of atmospheric particles from
1206 sulfuric acid, *Atmos. Chem. Phys.*, doi:10.5194/acp-20-7359-2020, 2020.
- 1207 Suikkanen, S., Laamanen, M. and Huttunen, M.: Long-term changes in summer phytoplankton communities
1208 of the open northern Baltic Sea, *Estuar. Coast. Shelf Sci.*, 71(3–4), 580–592,
1209 doi:10.1016/j.ecss.2006.09.004, 2007.
- 1210 Suikkanen, S., Pulina, S., Engström-Öst, J., Lehtiniemi, M., Lehtinen, S. and Brutemark, A.: Climate Change
1211 and Eutrophication Induced Shifts in Northern Summer Plankton Communities, *PLoS One*, 8(6), 1–10,
1212 doi:10.1371/journal.pone.0066475, 2013.
- 1213 Torn, K., Krause-Jensen, D. and Martin, G.: Present and past depth distribution of bladderwrack (*Fucus*
1214 *vesiculosus*) in the Baltic Sea, *Aquat. Bot.*, 84(1), 53–62, doi:10.1016/j.aquabot.2005.07.011, 2006.
- 1215 Väkevä, M., Hämeri, K., Puhakka, T., Nilsson, E. D., Hohti, H. and Mäkelä, J. M.: Effects of meteorological
1216 processes on aerosol particle size distribution in an urban background area, *J. Geophys. Res. Atmos.*,
1217 105(D8), 9807–9821, doi:10.1029/1999JD901143, 2000.
- 1218 Vanhanen, J., Mikkilä, J., Lehtipalo, K., Sipilä, M., Manninen, H. E., Siivola, E., Petäjä, T. and Kulmala, M.:
1219 Particle size magnifier for nano-CN detection, *Aerosol Sci. Technol.*, 45(4), 533–542,
1220 doi:10.1080/02786826.2010.547889, 2011.
- 1221 Wang, Z., Wu, Z., Yue, D., Shang, D., Guo, S., Sun, J., Ding, A., Wang, L., Jiang, J., Guo, H., Gao, J., Cheung,
1222 H. C., Morawska, L., Keywood, M. and Hu, M.: New particle formation in China: Current knowledge
1223 and further directions, *Sci. Total Environ.*, doi:10.1016/j.scitotenv.2016.10.177, 2017.
- 1224 Wang, Z. B., Hu, M., Yue, D. L., Zheng, J., Zhang, R. Y., Wiedensohler, A., Wu, Z. J., Nieminen, T. and Boy,
1225 M.: Evaluation on the role of sulfuric acid in the mechanisms of new particle formation for Beijing case,
1226 *Atmos. Chem. Phys.*, 11(24), 12663–12671, doi:10.5194/acp-11-12663-2011, 2011.
- 1227 Weber, R. J., McMurry, P. H., Mauldin, L., Tanner, D. J., Eisele, F. L., Brechtel, F. J., Kreidenweis, S. M.,
1228 Kok, G. L., Schillawski, R. D. and Baumgardner, B.: A study of new particle formation and growth
1229 involving biogenic and trace gas species measured during ACE I, *J. Geophys. Res. Atmos.*, 103(D13),
1230 16385–16396, doi:10.1029/97JD02465, 1998.



- 1231 Weber, R. J., McMurry, P. H., Mauldin, R. L., Tanner, D. J., Eisele, F. L., Clarke, A. D. and Kapustin, V. N.:
1232 New particle formation in the remote troposphere: A comparison of observations at various sites,
1233 *Geophys. Res. Lett.*, 26(3), 307–310, doi:10.1029/1998GL900308, 1999.
- 1234 Wimmer, D., Buenrostro Mazon, S., Elina Manninen, H., Kangasluoma, J., Franchin, A., Nieminen, T.,
1235 Backman, J., Wang, J., Kuang, C., Krejci, R., Brito, J., Goncalves Morais, F., Turnbull Martin, S.,
1236 Artaxo, P., Kulmala, M., Kerminen, V. M. and Petäjä, T.: Ground-based observation of clusters and
1237 nucleation-mode particles in the Amazon, *Atmos. Chem. Phys.*, 18(17), 13245–13264, doi:10.5194/acp-
1238 18-13245-2018, 2018.
- 1239 Yan, C., Yin, R., Lu, Y., Dada, L., Yang, D., Fu, Y., Kontkanen, J., Deng, C., Garmash, O., Ruan, J., Baalbaki,
1240 R., Schervish, M., Cai, R., Bloss, M., Chan, T., Chen, T., Chen, Q., Chen, X., Chen, Y., Chu, B.,
1241 Dällenbach, K., Foreback, B., He, X., Heikkinen, L., Jokinen, T., Junninen, H., Kangasluoma, J.,
1242 Kokkonen, T., Kurppa, M., Lehtipalo, K., Li, H., Li, H., Li, X., Liu, Y., Ma, Q., Paasonen, P., Rantala,
1243 P., Pileci, R. E., Rusanen, A., Sarnela, N., Simonen, P., Wang, S., Wang, W., Wang, Y., Xue, M., Yang,
1244 G., Yao, L., Zhou, Y., Kujansuu, J., Petäjä, T., Nie, W., Ma, Y., Ge, M., He, H., Donahue, N. M.,
1245 Worsnop, D. R., Veli-Matti, K., Wang, L., Liu, Y., Zheng, J., Kulmala, M., Jiang, J. and Bianchi, F.:
1246 The Synergistic Role of Sulfuric Acid, Bases, and Oxidized Organics Governing New-Particle
1247 Formation in Beijing, *Geophys. Res. Lett.*, doi:10.1029/2020GL091944, 2021.
- 1248 Yao, L., Garmash, O., Bianchi, F., Zheng, J., Yan, C., Kontkanen, J., Junninen, H., Mazon, S. B., Ehn, M.,
1249 Paasonen, P., Sipilä, M., Wang, M., Wang, X., Xiao, S., Chen, H., Lu, Y., Zhang, B., Wang, D., Fu, Q.,
1250 Geng, F., Li, L., Wang, H., Qiao, L., Yang, X., Chen, J., Kerminen, V. M., Petäjä, T., Worsnop, D. R.,
1251 Kulmala, M. and Wang, L.: Atmospheric new particle formation from sulfuric acid and amines in a
1252 Chinese megacity, *Science* (80-.), 361(6399), 278–281, doi:10.1126/science.aao4839, 2018.
- 1253 Yu, H., Ren, L., Huang, X., Xie, M., He, J. and Xiao, H.: Iodine speciation and size distribution in ambient
1254 aerosols at a coastal new particle formation hotspot in China, *Atmos. Chem. Phys.*, doi:10.5194/acp-19-
1255 4025-2019, 2019.
- 1256 Zhang, R., Wang, L., Khalizov, A. F., Zhao, J., Zheng, J., McGraw, R. L. and Molina, L. T.: Formation of
1257 nanoparticles of blue haze enhanced by anthropogenic pollution, *Proc. Natl. Acad. Sci. U. S. A.*,
1258 106(42), 17650–17654, doi:10.1073/pnas.0910125106, 2009.
- 1259 Zheng, G., Kuang, C., Uin, J., Watson, T. and Wang, J.: Large contribution of organics to condensational
1260 growth and formation of cloud condensation nuclei (CCN) in the remote marine boundary layer, *Atmos.*
1261 *Chem. Phys.*, doi:10.5194/acp-20-12515-2020, 2020.
- 1262
1263
1264
1265
1266



1300 Table 1: Timing and maximum concentration of SA, MSA and IA during local and burst/spike
1301 nucleation events during the study period

Dates	Type of Event	time of NPF (UTC+02:00 h)	SA (max) molec. cm ⁻³	MSA (max) molec. cm ⁻³	IA(max) molec. cm ⁻³
30.06.2019	Regional/ local	8:45-13:23 14:00-16:30	7.9 × 10 ⁶	5.6 × 10 ⁵	2.3 × 10 ⁶
30.07.2019	Regional/ local	7:45 -11:16	1.2 × 10 ⁷	1.2 × 10 ⁶	5.3 × 10 ⁶
11.08.2019	Ion Burst (Spike)	13:40-14:32	1.0 × 10 ⁷	1 × 10 ⁶	3.2 × 10 ⁷
14.08.2019	Ion Burst (Spikes)	8:00-8:20	4.2 × 10 ⁶	5.3 × 10 ⁵	8.5 × 10 ⁶
15.08.2019	Multiple Ion Bursts (Spikes)	6:00, 8:58, 14:00-16:00	6.4 × 10 ⁶ 6.3 × 10 ⁶ 7.0 × 10 ⁶	5.8 × 10 ⁵ 4.6 × 10 ⁵ 6.8 × 10 ⁵	2.5 × 10 ⁶ 3.1 × 10 ⁶ 1.5 × 10 ⁶

1302
1303
1304
1305
1306
1307
1308
1309
1310
1311
1312
1313
1314
1315
1316
1317
1318

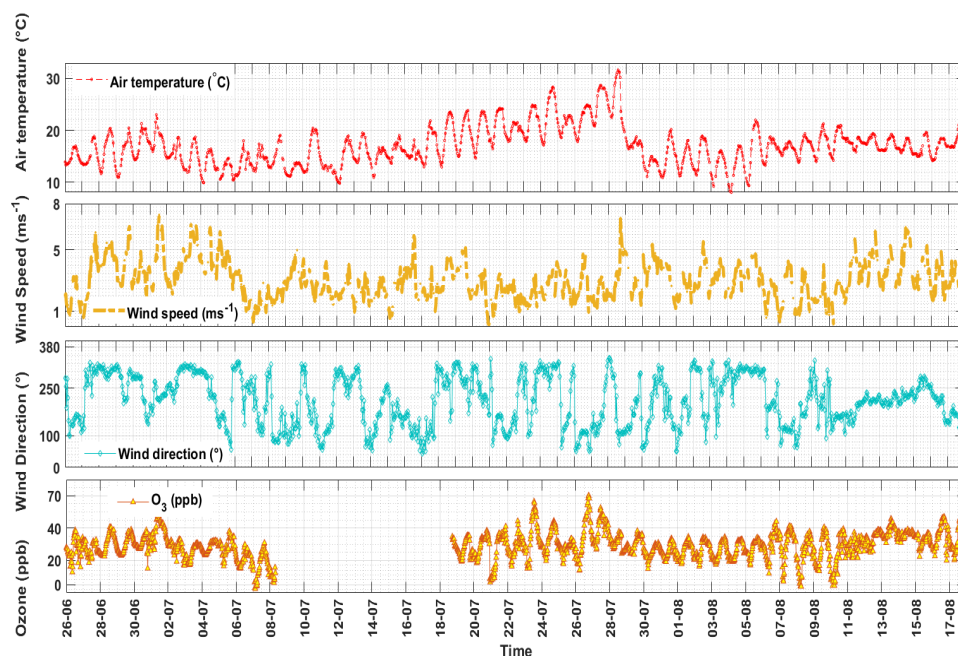


1319
1320



1321
1322 **Figure 1:** Map showing the two locations included in the study where instruments were operated
1323 (upper left panel). The yellow polygons on the left side of the measurement locations (on the lower
1324 right panel) shows forest/park with little or no traffic (West and Northwest, 300 m from the
1325 measurement site). The yellow double lines on the right of the measurement locations is the traffic
1326 area or the main road (E75) leading to the Helsinki city center (250 m east of the measurement site).
1327 The blue lines depict the coastline after which the lakes and coastal waters of Gulf of Finland start (1
1328 km to the east from the measurement site) © Google Earth 2019.

1329
1330
1331
1332
1333
1334
1335

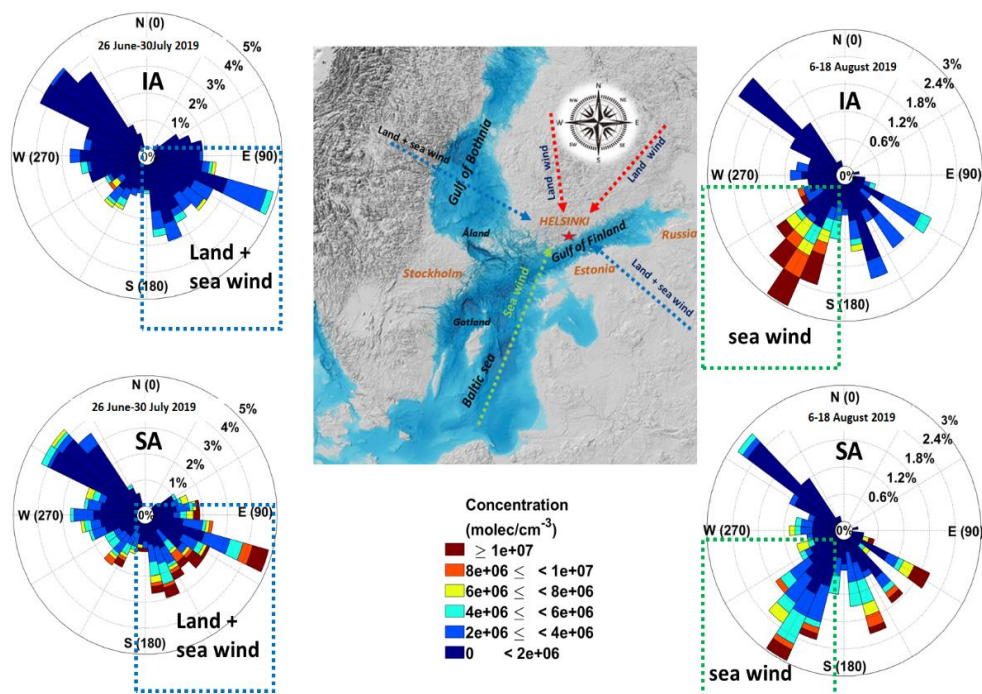


1336
1337
1338
1339
1340
1341
1342
1343
1344
1345
1346
1347
1348
1349
1350
1351
1352
1353
1354
1355

Figure 2: Time series of meteorological parameters and O₃ (data from SMEAR III station, 30-minute averaged) during the study period.



1356



1357

1358

1359 **Figure 3:** Windroses showing the variability in the concentration of gases with wind direction during
1360 the study period. Percentages on the concentric circles denote the frequency of winds from different
1361 directions. The spokes are color coded as per the concentration of the gas from the particular direction.
1362 The numbers in the parenthesis within the windroses refer to the wind direction in degrees.

1363

1364

1365

1366

1367

1368

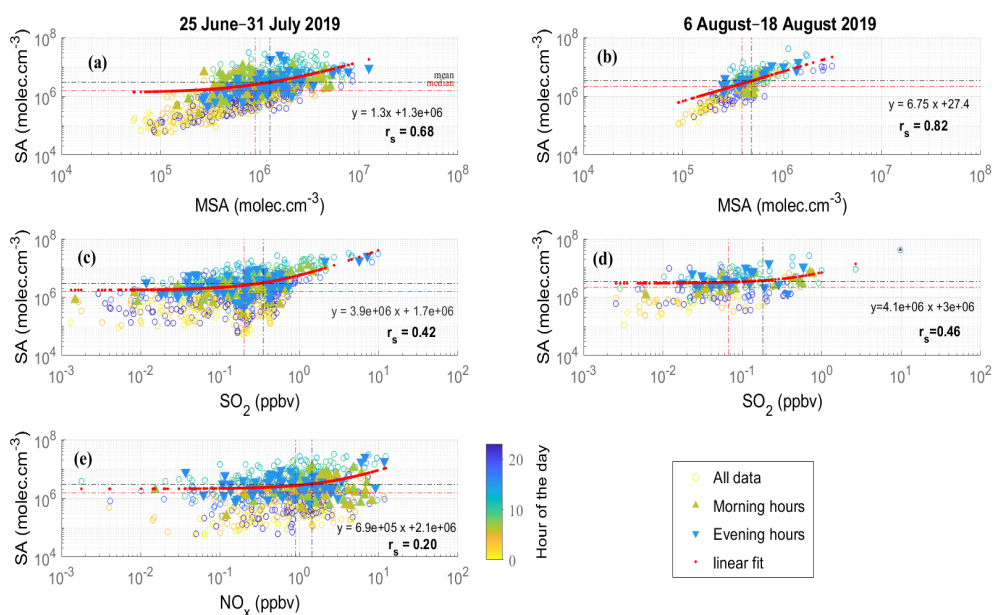
1369

1370

1371

1372

1373



1374

1375

1376 **Figure 4:** Correlation of SA with MSA (a,b), SO₂ (c,d) and NO_x (e) for June–July. The black dashed
1377 lines for both axis represent the mean of the gas concentration, red dashed line represent the median
1378 value the gas concentrations and red solid line represents the linear fit. Spearman's coefficient (r_s)
1379 was used to test the correlation, at significance level, 0.001. The circles represent data points at
1380 different hours of the day. The upward pointing green triangles represent the morning rush hours
1381 (6:00–8:00 h) and the downward pointing blue triangles represent the evening rush hours (15:00–
1382 17:00 h). The yellow hollow circles represent all data. NO_x data unavailable of August.

1383

1384

1385

1386

1387

1388

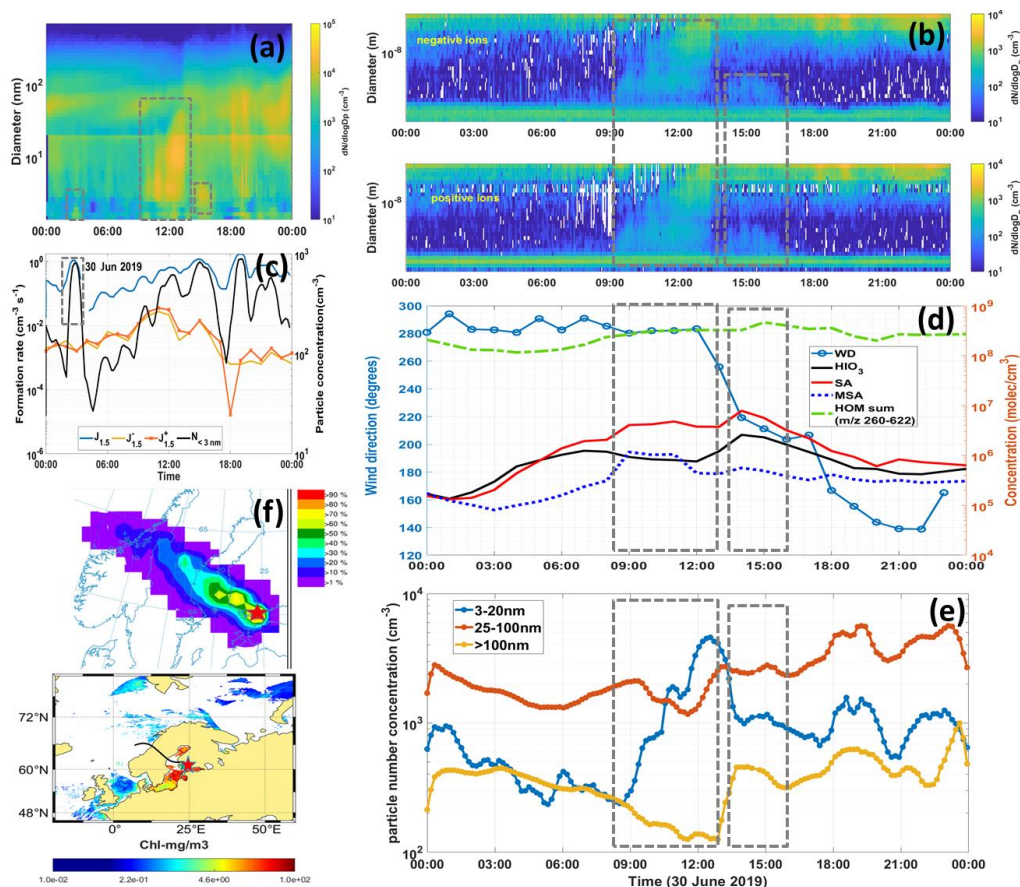
1389

1390

1391

1392

1393



1394

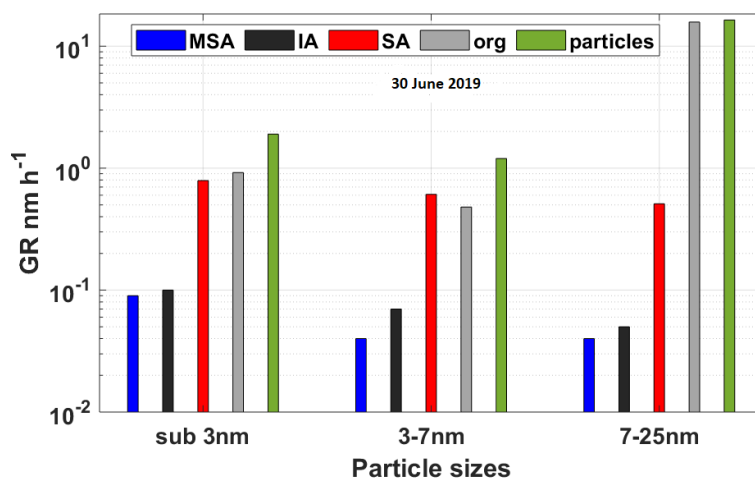
1395

1396 **Figure 5:** NPF Event (Regional and local events), 30 June 2019, the large dashed rectangle denotes
 1397 the regional event, the small dashed rectangles show local cluster formation events. (a) Number size
 1398 distribution of particles (data from PSM, NAIS and DMPS; size range: sub-3–100nm). (b) Charged
 1399 particles number size distribution (negative: upper, positive: lower) obtained from the NAIS. (c)
 1400 Diurnal variation of formation rates ($J_{1.5}$) of 1.5 nm particles and ions ($J_{1.5}^-$ and $J_{1.5}^+$) on the left axis
 1401 and particle number concentrations (1.5–3 nm) on the right axis. (d) Diurnal variation of HOMs SA,
 1402 IA and MSA with wind direction (WD). (e) The diurnal variation of particle concentration in
 1403 nucleation: 3–20 nm; aitken: 25–100 nm and accumulation: >100 nm mode particles during the event
 1404 (Data from DMPS). (f) Trajectory frequency plot (100 a.g.l, arrival time of trajectories at the
 1405 measurement site: 20:00 h) for 24 h back trajectory using GDAS meteorological input data (frequency
 1406 grid resolution: $1.0^\circ \times 1.0^\circ$) and Chl-*a* concentrations (MODIS); Black line shows the trajectory
 1407 direction and the red-star point denotes the measurement site.

1408



1409



1410

1411

1412 **Figure 6:** Particle growth rates calculated from the kinetic condensation of gases (data from CI-API-
1413 ToF) and the observed particle GRs (data from NAIS) in different size classes on 30 July 2019.

1414

1415

1416

1417

1418

1419

1420

1421

1422

1423

1424

1425

1426

1427

1428

1429

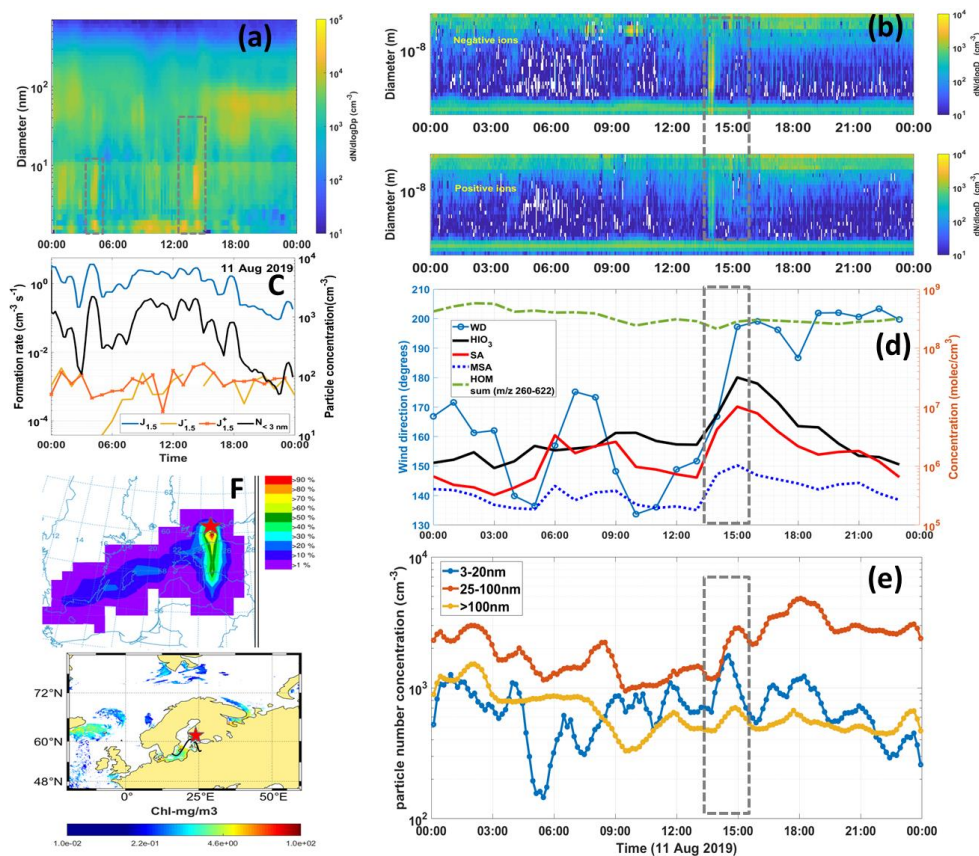
1430

1431

1432



1433



1434

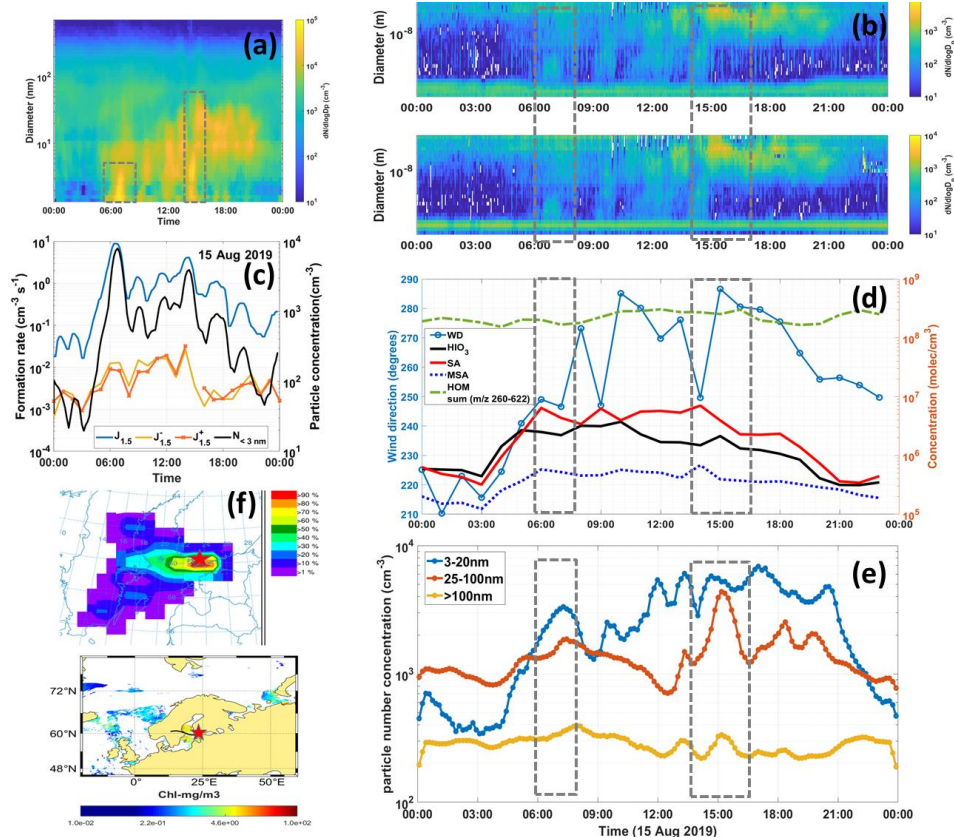
1435

1436 **Figure 7:** Burst/Event, 11 August 2019, The dashed grey rectangles denote the time stamp of the
 1437 nucleation events. (a) Number size distribution of particles (data from PSM, NAIS and DMPS; size
 1438 range: 1–100 nm). (b) Charged particles number size distribution (negative: upper, positive: lower)
 1439 obtained from the NAIS. (c) Diurnal variation of formation rates ($J_{1.5}$) of 1.5 nm particles and ions
 1440 ($J_{1.5}$ and $J_{1.5}^+$) and total number concentrations of particles (<3 nm, PSM). (d) Diurnal variation of
 1441 HOMs, SA, IA and MSA with wind direction (WD). (e) The diurnal variation of particle
 1442 concentration in nucleation (3–20 nm), Aitken (25–100 nm) and accumulation mode (>100 nm)
 1443 particles (DMPS data). (f) Trajectory frequency plot (100 a.g.l, arrival time of trajectories at
 1444 measurement site: 22:00 h) for 24 hour back trajectory using GDAS meteorological input data
 1445 (frequency grid resolution: $1.0^\circ \times 1.0^\circ$) and Chl-*a* concentrations (MODIS); Black line shows the
 1446 trajectory direction and the red star point denotes the measurement site.

1447



1448



1449

1450

1451 **Figure 8:** Multiple Burst/Spikes, 15 August 2019, The dashed grey rectangles denote the time stamp
 1452 of the nucleation events. (a) Number size distribution of particles (data from PSM, NAIS and DMPS;
 1453 size range: 1–100nm). (b) Charged particles number size distribution (negative: upper, positive:
 1454 lower) obtained from the NAIS. (c) Diurnal variation of formation rates ($J_{1.5}$) of 1.5 nm particles and
 1455 ions ($J_{1.5}^-$ and $J_{1.5}^+$) and total number concentrations of particles (<3 nm, PSM). (d) Diurnal variation
 1456 of HOMs SA, IA and MSA with wind direction (WD). (e) The diurnal variation of particle
 1457 concentration in nucleation (3–20 nm), Aitken (25–100 nm) and accumulation mode (>100 nm)
 1458 particles (DMPS data).(f) Trajectory frequency plot (100 a.g.l, arrival time of trajectories at the
 1459 measurement site: 22:00 h) for 24 h back trajectory using GDAS meteorological input data (frequency
 1460 grid resolution: $1.0^\circ \times 1.0^\circ$) and Chl-a concentrations (MODIS); Black line shows the trajectory
 1461 direction and the red-star point denotes the measurement site.

1462

1463